19. Nisbet-Brown E, Olivieri NF, Giardina PJ, et al. Effectiveness and safety of ICL670 in iron-loaded patients with thalassaemia: a randomised, double-blind, placebo-controlled, dose-escalation trial. Lancet. 2003;361:1597–602.
20. Piga A, Galanello R, Cappellini MD, et al. Phase II study of ICL670, an oral chelator, in adult thalassaemia patients with transfusional iron overload: efficacy, safety, pharmacokinetics (PK) and pharmacodynamics (PD) after 18 months of therapy. Blood. 2003;102: abstr 412.
21. Vichinsky E. Clinical application of deferasirox: practical patient management. Am J Hematol. 2008;83:398–402.

Research Paper

Vitamin K2 induces autophagy and apoptosis simultaneously in leukemia cells

Tomohisa Yokoyama,[1,5,†] Keisuke Miyazawa,[1, †,*] Munekazu Naito,[2] Juri Toyotake,[1] Testuzo Tauchi,[1] Masahiro Itoh,[2] Akira Yuo,[3] Yuho Hayashi,[4] Maria-Magdalena Georgescu,[4] Yasuko Kondo,[5] Seiji Kondo[5] and Kazuma Ohyashiki[1]

[1]First Department of Internal Medicine; Tokyo Medical University; [2]Department of Anatomy; Tokyo Medical University; Tokyo, Japan;[3]Department of Hematology; Research Institute; International Medical Center of Japan; Tokyo, Japan; [4]Department of Neuro-Oncology and [5]Department of Neurosurgery; The University of Texas MD Anderson Cancer Center; Houston, Texas USA

†These authors contributed equally to this work.

Vitamin K2 (menaquinone-4: VK2) is a potent inducer for apoptosis in leukemia cells in vitro. HL-60*bcl-2* cells, which are derived from a stable transfectant clone of the human *bcl-2* gene into the HL-60 leukemia cell line, show 5-fold greater expression of the Bcl-2 protein compared with HL-60*neo* cells, a control clone transfected with vector alone. VK2 induces apoptosis in HL-60*neo* cells, whereas HL-60*bcl-2* cells are resistant to apoptosis induction by VK2 but show inhibition of cell growth along with an increase of cytoplasmic vacuoles during exposure to VK2. Electron microscopy revealed formation of autophagosomes and autolysosomes in HL-60*bcl-2* cells after exposure to VK2. An increase of acid vesicular organelles (AVOs) detected by acridine orange staining for lysosomes as well as conversion of LC3B-I into LC3B-II by immunonoblotting and an increased punctu-ated pattern of cytoplasmic LC3B by fluorescent immunostaining all supported induction of enhanced autophagy in response to VK2 in HL-60*bcl-2* cells. However, during shorter exposure to VK2, the formation of autophagosomes was also prominent in HL-60*neo* cells although nuclear chromatin condensations and nuclear fragments were also observed at the same time. These findings indicated the mixed morphologic features of apoptosis and autophagy. Inhibition of autophagy by either addition of 3-methyladenine, siRNA for Atg7, or Tet-off Atg5 system all resulted in attenuation of VK2-incuded cell death, indicating autophagy-mediated cell death in response to VK2. These data demonstrate that autophagy and apoptosis can be simultaneously induced by VK2. However, autophagy becomes prominent when the cells are protected from rapid apoptotic death by a high expres-sion level of Bcl-2.

*Correspondence to: Keisuke Miyazawa; First Department of Internal Medicine; Tokyo Medical University; 6-7-1, Nishishinjuku; Shinjuku-ku, Tokyo 160-0023 Japan; Tel.: +81.3.3342.6111, ext. 5985; Fax: +81.3.5381.6651; Email: miyazawa@tokyo-med.ac.jp

Introduction

The vitamin K family contains both natural and synthetic forms, the former including phytonadione (VK1) and the menaquinone series (VK2), and the latter including menadione (VK3). Recent studies have reported that VK2 can exert cell growth-inhibitory effects in various human cancer cells including leukemia, lung cancer and hepatocellular carcinoma (HCC) cells.[1-5] We previously reported that this cytotoxic effect of VK2 appears to be selective to leukemic blasts with almost no effects on normal hematopoietic progenitor cells.[2,6] This suggests a therapeutic advantage for using VK2 in therapy for leukemia. Several recent clinical trials demonstrated that oral administration of VK2 reduced leukemic blasts in acute myeloid leukemia (AML) and improvement of cytopenias in myelodysplastic syndromes (MDS), and also decreased the development and recur-rence rates of HCC, thus improving the overall survival of patients with HCC.[7-10] Although the precise mechanism of how VK2 exerts its growth-inhibitory effects in cancer cells has not been determined, VK2 has been reported to be a potent inducer of apoptosis in various tumor cells including leukemic cells in vitro.[2,3,11-15]

Apoptosis is an evolutionally conserved, orchestrated cell-death process characterized by membrane-blebbing, DNA fragmentation, and the formation of distinct apoptotic bodies that contain compo-nents of the dead cell.[16,17] This process occurs without membrane breakdown and does not elicit an inflammatory response. Apoptotic bodies are eventually removed by phagocytic cells. Central to this apoptotic process are a group of caspases, which effect the destruction of the cell in an orderly fashion.[17] Extensive evidence suggests that therapeutic effects of various anti-cancer reagents and of radiation are mediated though apoptosis of cancer cells.[18] However, another type of caspase-independent cell death designated autophagic cell death has recently been suggested in some cancer cells in response to anticancer therapy.[19-22]

Autophagy is also an evolutionally conserved membrane trafficking process that leads to degradation of cytosolic proteins and organelles by lysosomes.[23,24] Cytosol and organelles such as mitochondria and endoplasmic reticulum are engulfed into double-membraned vesicles called autophagosomes. Fusion subsequently occurs between the

autophagosomes and lysosomes to form autolysosomes in which the cargo of the autophagosome is degraded by lysosomal hydrolases. Autophagy is induced above basal levels in response to nutrient deprivation or trophic factor withdrawal, and it sustains metabolism through the targeted catabolism of long-lived proteins. Thus, autophagy acts as a self-limited survival mechanism.[23,24] A group of genes known as Atg genes, which are conserved from yeast to humans, have been found to regulate autophagy.[25] A number of studies have reported that autophagy is activated in cancer cells derived from breast, colon, prostate and brain in response to various anticancer therapies.[21,22] Since inhibition of autophagy results in suppression of cancer cell death by anti-cancer reagents, autophagy is suggested to be a potential contributor to non-apoptotic programmed cell death.[19,21] When cell death involves autophagy, it is now designated as type II programmed cell death (PCD) or autophagic cell death, in contrast to apoptosis, which is referred to as type I PCD.[19,21] The morphological and biochemical features of autophagic cell death and apoptosis are generally distinct. In autophagic cell death, unlike apoptotic cell death, caspases are not activated, and neither DNA degradation nor nuclear fragmentation is apparent. Instead, autophagic cell death is characterized by degradation of the Golgi apparatus, polyribosomes and endoplasmic reticulum before nuclear destruction, whereas these organelles are preserved in apoptosis.[19,21] However, the involvement of autophagy in programmed cell death is still controversial, probably because the molecule(s) which execute cell death in autophagy have not been identified.[20-22]

We have previously reported that overexpression of Bcl-2 in a leukemia cell line resulted in resistance against VK2-induced apoptosis but these cells still underwent differentiation via G_1 arrest.[12] In addition, downregulation of Bcl-2 was reported to cause autophagy of HL-60 cells in a caspase-independent manner.[26] It has also been reported that Bcl-2 negatively regulates Beclin 1-depemdent autophagy and Beclin 1-dependent autophagic cell death.[27] All these data suggest the involvement of Bcl-2 in some autophagic signaling and also imply some direct or indirect interaction between mitochondria and lysosomes.[28]

In the present study, we investigated whether autophagy is involved in VK2-induced leukemic cell death using subclones of HL-60 cell line with higher and lower expression levels of the Bcl-2 protein. Our data demonstrated that both autophagy and apoptosis are simultaneously induced after VK2 treatment, but autophagy become more evident and detectable when the cells are protected from apoptosis.

Results

Bcl-2 abolished VK2-induced apoptosis but had little effect on VK2-induced growth inhibition in HL-60 cells. We have reported that treating the primary cultured leukemic cells and leukemic cell lines with 1–10 µM of VK2 for 48 to 96 hr induces apoptosis in vitro, and that the expression levels of Bcl-2 determine whether the leukemic cells to undergo apoptosis or differentiation.[2,12]

Immunoblotting with anti-Bcl-2 mAb revealed that HL-60*bcl-2* cells, which are stably transfected with human *bcl-2*, expresse Bcl-2 at a five-fold higher level than HL-60*neo* control cells (Fig. 1A). There was no difference in growth rate, morphology, and antigen expressions among the parental HL-60, HL-60*neo*, and HL-60*bcl-2* cells (data not shown). Thereafter, cell growth inhibition was assessed after 96-hr exposure to VK2 (menaquinone-4) at various

concentrations. As shown in Figure 1B, VK2 inhibited HL-60 cell growth in a dose-dependent manner. HL-60*bcl-2* cells were less sensitive as compared with HL-60*neo* cells; the concentrations for the 50% growth inhibition (IC_{50}) were 6 µM for HL-60*neo* and 14 µM for HL-60*bcl-2* cells, respectively.[12] As previously reported in other leukemic cell lines and primary cultured leukemic cells,[2,11,13] treatment with 10 µM of VK2 for 72 hr potently induced apoptosis of HL-60*neo* cells as assessed by morphology, depolarization of mitochondrial membrane potential, and annexin V staining (Fig. 1C–E). In contrast, apoptosis induction by VK2 treatment was significantly suppressed in HL-60*bcl-2* cells (Fig. 1D and E), although the inhibition of cell growth was still detectable, and extended exposure to VK2 induced cell death in HL-60*bcl-2* cells (Fig. 1B). We therefore investigated whether the autophagy or non-apoptotic cell death occurred in HL-60*bcl-2* cells after treatment with VK2.

Induction of autophagy in HL-60neo/*bcl-2* cells by VK2. Since cytoplasmic vesicles became evident in HL-60*bcl-2* cells after treatment with VK2 (Fig. 1C), we first performed electron microscopy to determine whether VK2 induces autophagy in HL-60*bcl-2* cells and compared the results with those obtained with HL-60*neo* cells. As shown in Figure 2A (upper right), the nuclear degeneration and multiple chromatin bodies, which are characteristic features for the cells undergoing apoptosis, were observed in HL-60*neo* cells treated with 10 µM of VK2 for 72 hr. In contrast, numerous autophagic vacuoles and empty vacuoles were observed in HL-60*bcl-2* cells under the same conditions (Fig. 2B; upper right and lower). Most of the autophagosomes contained lamellar structures with residual digested materials. These results indicated that HL-60*bcl-2* cells treated with VK2 undergo autophagy.

It was previously reported that during amino acid starvation, LC3 becomes localized to form isolated membrane following formation of autophagosome membranes.[34] Therefore detection of the punctuated pattern of cytosolic LC3 indicates the involvement of LC3 for autophagosome formation. This phenomenon has been used as method for monitoring autophagy.[35] To further confirm the involvement of LC3 in VK2-induced autophagy, we performed fluorescent immunocytostaining of HL-60neo/*bcl-2* cells with anti-LC3B Ab and subsequent counter staining with DAPI for the detection of nuclei. As shown in Figure 3A and B, untreated HL-60*neo* and HL-60*bcl-2* cells both showed diffuse distribution of green fluorescence and no fragmented nuclei, whereas treatment with VK2 increased the punctuated pattern of LC3B in HL-60*bcl-2* cells, representing autophagic vacuoles. HL-60*neo* cells with fragmented nuclei showed no punctuated pattern of LC3B. However, in a minor population of HL-60*neo* cells without fragmented nuclei, the punctuated pattern of LC3B staining was detected. Among the cells without nuclear fragments during 72 hr-treatment with 10 µM of VK2, the percentage showing the punctuated pattern of LC3B increased in HL-60*neo* cells as well as HL-60*bcl-2* cells (Fig. 3B). This indicates that autophagy can be detected not only HL-60*bcl-2*cells but also HL-60*neo* cells. Within 48 hrs of exposure to VK2, autophagy induction was rather prominent in HL-60*neo* cells as compared with HL-60*bcl-2* cells.

Simulations induction of both apoptosis and autophagy in HL-60 cells after treatment with VK2. The data shown above suggested that both autophagy and apoptosis appear to be induced in response to VK2 in HL-60*neo* cells. For semi-quantitative assessment of the induction of autophagy, we examined the development of acid
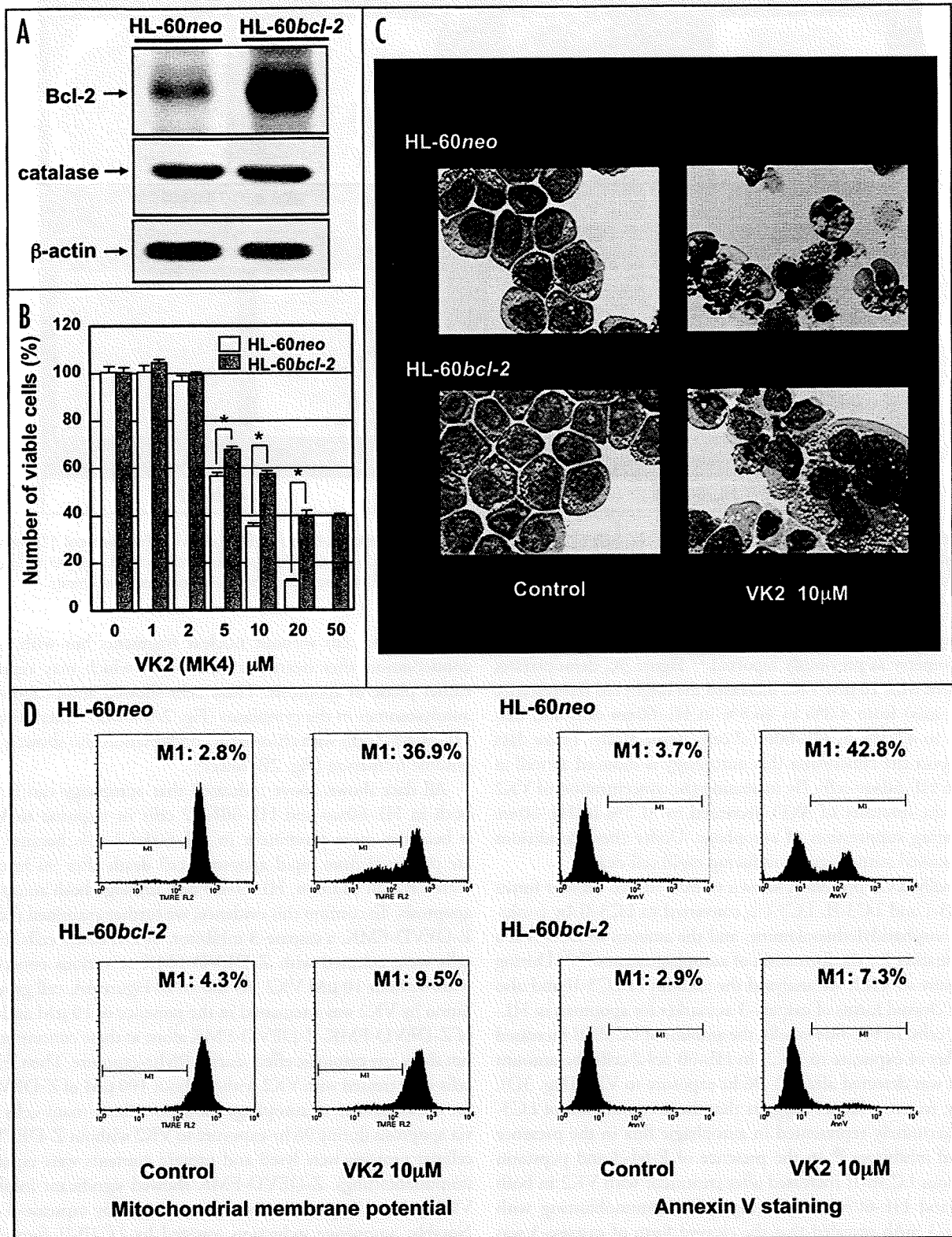
Figure 1. Inhibition of cell growth and induction of apoptosis after treatment with VK2 in HL-60 cells. (A) Expression of Bcl-2 and catalase in HL-60neo and HL-60bcl-2 cells: Cellular proteins were lysed and separated by 15% SDS-PAGE for Bcl-2 and 11.25% SDS-PAGE for catalase and β-actin, and immunoblotted with anti-human Bcl-2 mAb, anti-catalase rabbit mAb, or anti-β-actin Ab, respectively. (B) Cell growth inhibition in response to VK2 in HL-60neo/HL-60bcl-2 cells: Cells were cultured in the presence of various concentrations of VK2 (0.1–50 μM) for 72 hr. The number of cells was assessed with the WST cell counting kit as described in Materials and Methods. Cell growth is expressed as a ratio to the untreated control cells. *p < 0.001. After 72 hr exposure to 10 μM of VK2, HL-60neo and HL-60bcl-2 cells were processed for (C) May-Grünwald-Giemsa staining for assessment of morphologic changes (original magnification x1,000), and flow cytometry for (D) mitochondrial membrane potential using TMRE, and (E) Annexin V staining as described in Materials and Methods.
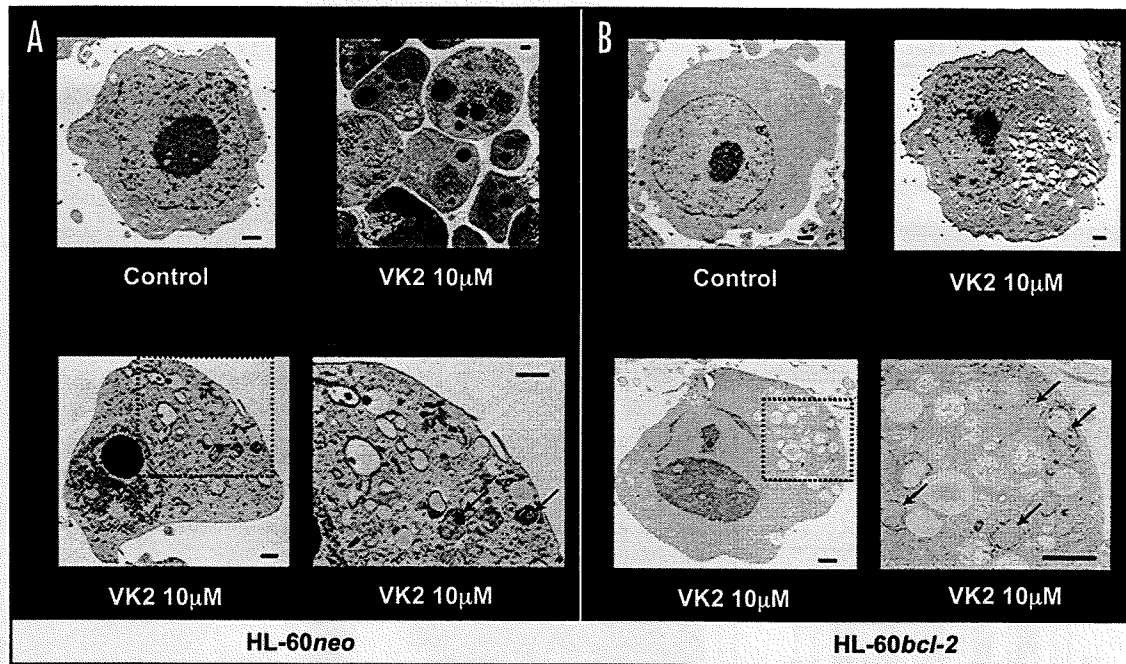
Figure 2. Ultrastructural features of HL-60neo/HL-60bcl-2 cells after exposure to VK2. HL-60neo/HL-60bcl-2 cells treated with or without 10 μM of VK2 for 72 hr. Then the cells were fixed, and the electron microscopy was performed. (A) HL-60neo cells: upper left; untreated control cells, upper right and lower; VK2-treated cells. (B) HL-60bcl-2 cells: upper left; untreated cells, upper right and lower; VK2-treated cells. Arrows indicate autolysosomes.

vesicular organelles (AVOs) with acridine orange staining followed by flow cytometry as previously reported.[29] Figure 3C demonstrates that treatment with 10 μM VK2 increased the bright red fluorescence intensity (y-axis) from 4.8% to 46.8% in HL-60neo cells and that from 4.7% to 47.3% in HL-60bcl-2 cells, respectively. These data further support the conclusion that autophagy is induced as well as apoptosis in HL-60neo cells. By increasing the concentration of VK2 at 20 μM, the intensity of AVO decreased to 31.5% in HL-60neo cells, indicating suppression of autophagy. Under these conditions apoptosis masked autophagy by inducing rapid cell death.

Additionally, LC3 protein is known to exist in two cellular forms such as LC3-I and LC3-II. LC3-I is converted to LC3-II by conjugation to phosphatidylethanolamine, and the amount of LC3-II is a good early marker for the formation of autophagosomes.[36,37] During 96 hr exposure to VK2, we analyzed the amount of LC3-II and also assessed the cleaved forms of caspase-3 as marker for apoptosis in HL-60neo/bcl-2 cells. In HL-60neo cells, the amount of LC3B-II increased within 48 hrs of exposure to VK2. In HL-60 bcl-2 cells the amount of LC3B-II was detected after 72–96 hr exposure to VK2 (Fig. 3D). In addition, recent evidence suggests that the accumulation of LC3-II is more accurately represented in autophagic flux in the presence of lysosomal inhibitors.[38] In the presence of E-64-d and pepstatin A, endogenous LC3B-II increased after treatment with VK2 in both HL-60neo and HL-60bcl-2 cells (Fig. 3E). Immunoblotting with anti-caspase-3 mAb revealed that the cleaved form of caspase-3 was significantly increased after treatment with VK2 for 48–96 hr in HL-60neo cells, whereas the cleaved caspase-3 was almost undetectable in HL-60bcl-2 cells during the 96 hr-exposure to VK2 (Fig. 3D). These results demonstrated that both autophagy and apoptosis occurred at the same time in HL-60neo cells. In addition, autophagy was induced earlier in HL-60neo cells than in HL-60bcl-2 cells during exposure to VK2. This was further confirmed by electron microscopy

of HL-60neo cells without nuclear fragments but with chromatin condensation after treatment with VK2, which may represent the earlier phase of apoptosis. These cells showed autophagosomes and autolysosomes in the cytoplasm (Fig. 2A; lower). Interestingly, some HL-60bcl-2 cells with chromatin condensation also showed autophagosome formation (Fig. 2B; lower).

All data shown above indicated that autophagy can be induced both in HL-60neo and HL-60bcl-2 cells in response to VK2, but it becomes more prominent in HL-60bcl-2 cells because the cells are protected from rapid apoptotic cell death after 96 hr-treatment with VK2. In addition, HL-60neo cells undergo both autophagy and apoptosis. To confirm this evidence, we further examined the effect of Z-DEVD-FMK, a caspase-3 inhibitor, in HL-60neo cells. HL-60neo cells were cultured with Z-DEVD-FMK at various concentrations with/without 10 μM VK2. As shown in Figure 4A, cell growth inhibition by VK2 was attenuated in the presence of 10 μM and 100 μM of Z-DEVD-FMK. Z-DEVD-FMK alone at these concentrations did not show any cytotoxic effect during 96 hr-exposure. Then, HL-60neo cells were treated with VK2 with/without 100 μM of Z-DEVD-FMK for the assessment of autophagy induction. Since many cells were lost via apoptosis during 96 hr-exposure to VK2 without Z-DEVD-FMK, cellular proteins were lysed and protein contents were equalized for immunoblottings. Z-DEVD-FMK showed significant inhibition of VK2-induced caspase-3 activation as assessed by capsease-3 cleavage. Notably, autophagy induction assessed by LC3B-II formation was significantly enhanced in the presence of Z-DEVD-FMK after 96 hr exposure to VK2 (Fig. 4B). These data also supported that autophagy becomes more prominent by blocking apoptotic cell death.

Mixed morphologic feature of autophagy and apoptosis in HL-60bcl-2 cells. The data shown above led us to further examine the morphologic features of HL-60bcl-2 and HL-60neo cells in detail after exposure to VK2.
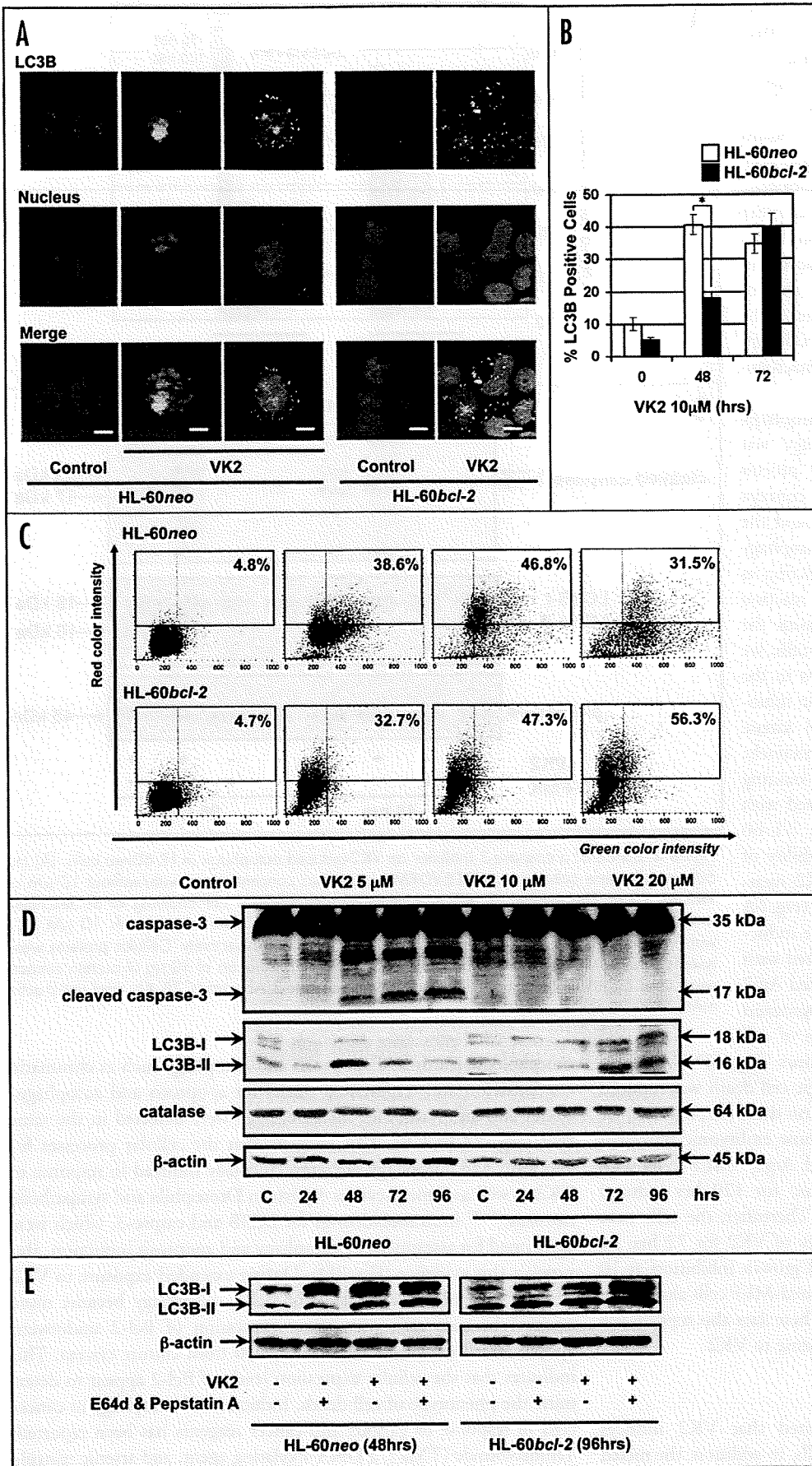
Figure 3. Induction of autophagy in response to VK2 in HL-60neo/HL-60bcl-2 cells. *Involvement of LC3B in VK2-induced autophagy:* After exposure to 10 µM VK2 for 48 and 72 hr, the cells were processed for fluorescent immunocytostaining with anti-LC3B Ab and counterstaining with DAPI for nucleus as described in Materials ant Methods. (A) HL-60neo/bcl-2 cells (original magnification x 1,000). (B) Quantification of the cells showing the punctuated pattern of LC3B staining, which marks cells with autophagosome formation. One hundred cells were assessed and ratios for the cells showing the punctuated pattern of LC3B staining were expressed. Results shown are the means ± SD from the results of three independent experiments. *p < 0.001. *Development of acidic vesicular organelles (AVOs) after VK2 treatment:* (C) After staining the cells with acridine orange, AVOs were quantified using flowcytometer in HL-60neo (upper) and HL-60bcl-2 (lower) treated with or without VK2 (5 µM, 10 µM or 20 µM) for 72 hr. X-axis, green color intensity; Y-axis, red color intensity. *Expression of isoforms of LC3B and caspase-3:* (D) Cellular proteins were lysed at the indicated time after incubation with or without 10 µM of VK2. Proteins were separated by either 11.25% or 15% SDS-PAGE. Aliquots of 40 µg of protein extracts were used for immunoblotting using anti-caspase-3 and anti-LC3B Abs, respectively. The anti-β-actin mAb was used for protein-loading equivalence. *Expression of isoforms of LC3B in the presence and absence of protease inhibitors:* (E) After treatment with 10 µM of VK2 for 44 hrs in HL-60neo and for 92 hrs in HL-60bcl-2 cells, cells were further cultured with/without protease inhibitors, E-64-d (10 µg/ml) and pepstatin A (10 µg/ml) in the presence of VK2 for 4 hrs. Cellular proteins were lysed and immunoblotted with anti-LC3B Ab.

After exposure to VK2 for 96 hr, HL-60*bcl-2* cells showed an increased percentage of fragmented nuclei compared to 72 hr treatment. Intriguingly, the morphologic findings in HL-60*bcl-2* cells undergoing apoptosis were different from those in HL-60*neo* cells; each nuclear fragment appeared to be encapsulated by vesicles resulting in the formation of a "sunny side-up" appearance (Fig. 5A). A "sunny side-up" appearance was also observed in HL-60*neo* cells treated with VK2 in the presence of a caspase-3 inhibitor, Z-DEVD-FMK. Extended exposure to VK2 up to 6 days resulted in the disappearance

of this characteristic feature and the appearance of the typical apoptotic bodies like in HL-60*neo* cells treated with 72 hr exposure to VK2 (Fig. 5B). Therefore, this morphologic change in HL-60*bcl-2* cells seems to be an early phase of cells undergoing apoptosis. To investigate whether the "sunny side-up" feature is macroautophagy of nuclear fragments, we examined the VK2 treated HL-60*bcl-2* cells by electron microscopy. Fragmented nuclei with condensed chromatin appeared to be surrounded by double-membrane (Fig. 5C). However, fluorescent immunocytostaining with anti-LC3B Ab showed that nuclear fragments were not surrounded by punctuated LC3B. Therefore, "sunny side-up" feature does not appear to represent the macroautophagy of nuclear fragments.

The biological roles of VK2-induced autophagy in HL-60*neo*/*bcl-2* cells. Since autophagy was initially recognized as a cellular survival process under amino acid starvation,[23,24] the concept of autophagic cell death as type II PCD and the significance of cancer treatment-induced autophagy is a subject of debate. Autophagy may function as an anti-cancer effect or a cytoprotective reaction against the cytotoxic reagents.[20-22] To assess the role of VK2-induced autophagy in HL-60 cells, we attempted to block the autophagic process in the presence or absence of VK2 using 3-MA, an inhibitor of class III phosophatidyl-inositol-3 kinase (PI3K),[31] and siRNA against Atg7, respectively. Treatment with 3-MA suppressed the PI-staining positive cells in HL-60*neo*/*bcl-2* cells treated with VK2. 3-MA alone showed no effect on HL-60 cell growth. In addition, the decreased viability of HL-60*neo* and HL-60*bcl-2* cells after VK2 treatment was reversed in the presence of 3-MA (Fig. 6A and B). Furthermore, 3-MA suppressed the induction of AVOs in HL-60*neo*/*bcl-2* cells treated with VK2 (Fig. 6C). siRNA effectively suppressed Atg7 expression in HL-60neo/*bcl-2* cells. Suppression of Atg7 resulted in significant attenuation of cell growth inhibition by VK2 in both cell lines (Fig. 6D). All these data support the conclusion that autophagic cell death was induced after treatment with VK2. To further confirm this interpretation, we used the Tet-off system with an Atg5^{-/-} mouse embryonic fibroblast (MEF) cell line.[33] Pretreatment of Tet-off Atg5^{-/-} MEF cells with 10 ng/ml doxycycline hydrochloride (Dox) for 120 hrs induced complete suppression of Atg5 expression. Thereafter, the cells were further cultured in the presence or absence of VK2 for 72 hrs. As shown in Figure 7, the VK2- induced cell growth inhibition at 10 μM was significantly attenuated in Dox treated-MEF cells along with suppression of the induction of LC3B-II. These data also support the occurrence of autophagic cell death in response to VK2.

Discussion

In the present study, we demonstrated that VK2 induces autophagy as well as apoptosis in HL-60 cells. In addition, the mixed
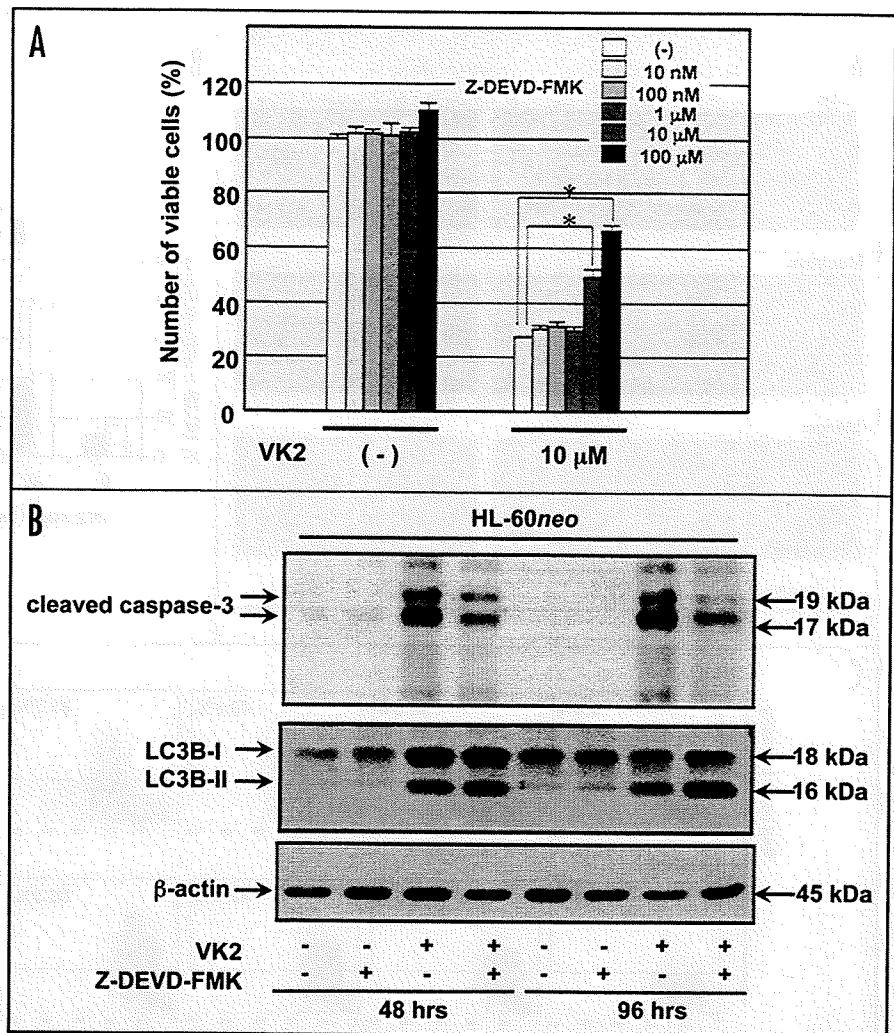

Figure 4. Effects of a caspase-3 inhibitor on VK2-induced autophagy in HL-60neo cells. (A) HL-60neo cells were cultured with Z-DEVD-FMK at various concentrations with/without 10 μM of VK2 for 96 hr. The number of cells was assessed with the WST cell counting kit as described in Materials and Methods. *p < 0.001. (B) HL-60neo cells were treated with 10 μM VK2 with/without 100 μM of Z-DEVD-FMK for 48 hr and 96 hr, respectively. Cellular proteins were lysed and separated by either 11.25% or 15% SDS-PAGE. Aliquots of 40 μg of protein extracts were used for immunoblotting using anti-cleaved caspase-3 Ab, anti-LC3B Ab, and anti-β-actin mAb, respectively.

morphologic features of apoptosis and autophagy such as chromatin condensation and fragmented nuclei for apoptosis and autophagosomes and autolysosomes for autophagy were detected in the same cells (Fig. 2A and B). This suggests that the cellular processes for apoptosis and autophagy are simultaneously induced in response to VK2 as well as some previous reports in Drosophila and sympathetic neurons.[39,40] Immunoblottings for LC3B and caspse-3, which were performed for assessment of autophagy and apoptosis induction, also support this evidence (Fig. 3D). During extended exposure to VK2 in cells with higher expression of Bcl-2, autophagy became more evident, because cells with lower expression of Bcl-2 underwent apoptotic cell death and were eliminated from culture system. This indicates that the cellular expression levels of Bcl-2 appear to determine the phenotype of cell death. Induction of autophagy in cancer cells in response to various anti-cancer reagents has been reported: Temozolomide (TMZ), a DNA alkylating agent, and arsenic trioxide
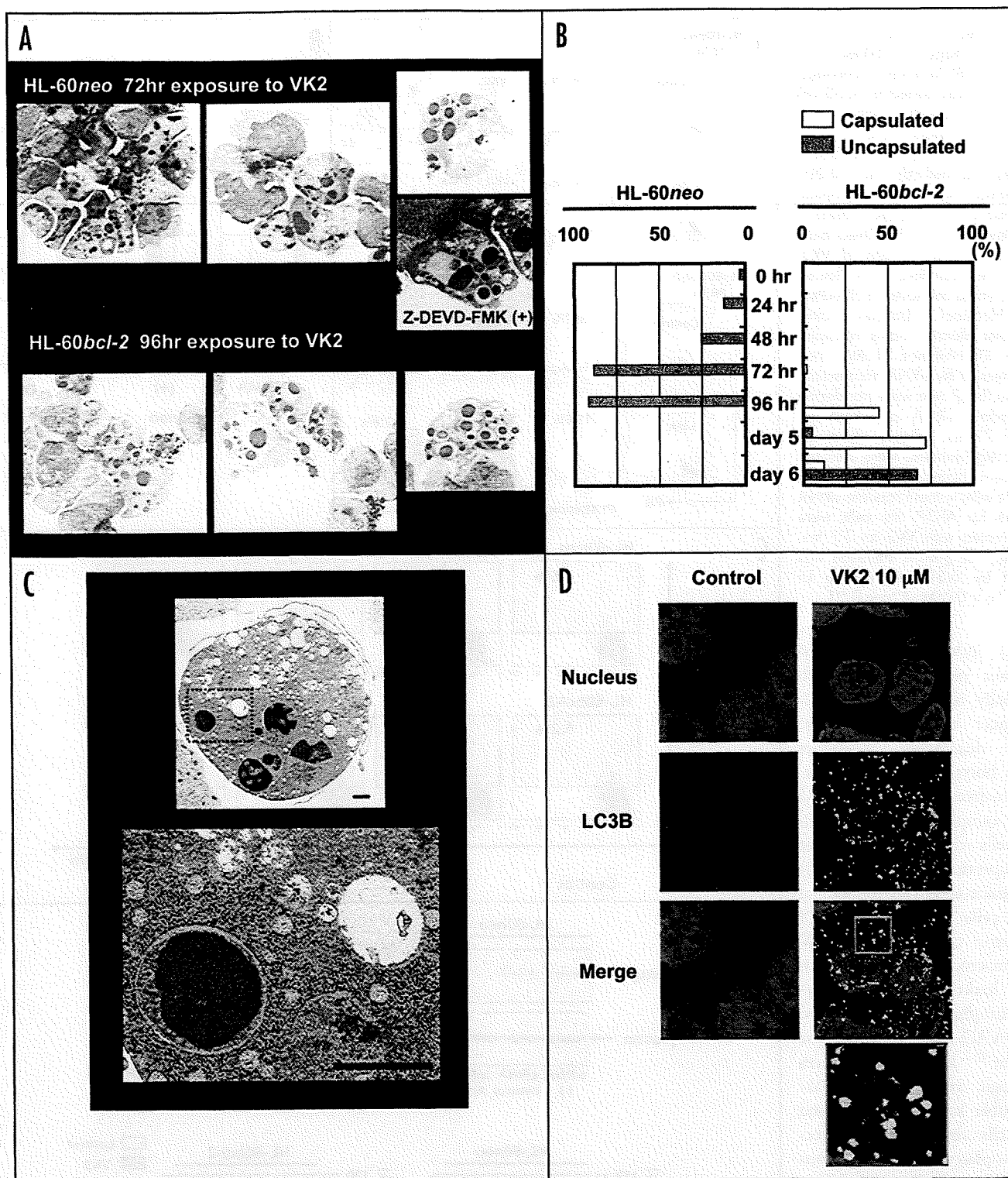
Figure 5. Capsulated fragmented nuclei in HL-60bcl-2 cells after treatment with VK2. (A) Morphological features of HL-60neo after 72 hr-treatment with VK2 (10 μM) with/without Z-DEVD-FMK (100 μM) and of HL-60bcl-2 cells after 96 hr-treatment with VK2. May-Grünwald-Giemsa staining, original magnification x 1,000. (B) Percentages of HL-60 cells with apoptotic bodies containing either capsulated nuclear fragments or uncapsulated nuclear. After treatment HL-60neo/bcl-2 cells with 10 μM of VK2 for various length of time, morphologic changes were assessed in 100 cells after May-Grünwald Giemsa stain as well as Figure 4A. (This is one of representative result from 3 separate experiments.) (C) Electron microscopy of HL-60bcl-2 cells after treatment with 10 μM VK2 for 96 hr. (D) Fluorescent immunocytostaining with anti-LC3B Ab in HL-60bcl-2 cells after 96 hr-treatment with 10 μM VK2. Fluorescent immunocytostaining with anti-LC3B Ab (original magnification x 1,000) was performed as described in Figure 3A and C, respectively. The slides stained with anti-LC3B Ab were monitored using Zeiss LSM510 confocal microscope (Original magnification x 600).

Figure 6. Effects of inhibition of VK2-induced autophagy in HL-60neo/bcl-2 cells. (A and B) To inhibit autophagy, 2 mM 3-MA was added to HL-60 cell cultures for 72 hr with or without VK2. Viable cell numbers were assessed using a flow cytometer as described in Materials and Methods. *p < 0.001 (C) Treatment with 3-MA suppressed the induction of acidic vesicular organelles (AVOs) in HL-60neo/bcl-2 cells treated with 10 μM of VK2. AVOs were quantified with fluorescence-activated cell sorter in HL-60neo (upper)/HL-60bcl-2 (bottom). x-axis, green color intensity; y-axis, red color intensity. (D) Inhibition of Atg7 protein expression by siRNA transfection: HL-60neo/bcl-2 cells were transfected with random siRNA or siRNA for Atg7 for 72 hrs. Relative expression levels of Atg7 proteins were assessed by western blotting. (upper). After treatment with/without random siRNA or siRNA for ATG7, the cells were further treated with VK2 for 72 hrs. Thereafter, cell growth inhibition was assessed by WST cell counting kit (lower). *p < 0.001, **p < 0.05.

(As_2O_3) induce autophagy of malignant glioma cells, which are usually refractory to various anti-cancer therapies.[30,41] The histone deacetylase inhibitors sodium butyrates and suberoyla-nilide hydeoxamic acid (SAHA) induce autophagic cell death in HeLa cells which overexpress the anti-apoptotic protein Bcl-X$_L$, but they induce apoptosis in parental HeLa cells.[42] Murine L929 fibroblastic cells, murine RAW 264.7 macrophages, and human U937 leukemia cells underwent autophagy after treatment with z-VAD-fmk, a pancaspase inhibitor.[43] Etoposide induces autophagic cell death in Bax/Bak-double knockout MEF, and these cells also undergo protective autophagy under conditions of nutrition depletion.[44] These conditions for induction of autophagy by cytotoxic stimuli include cellular resistance against apoptosis or protection from apoptosis. Our observations showing autophagy in HL-60bcl-2 rather than HL-60neo cells meet these conditions. However, our data also demonstrated that apoptotic and
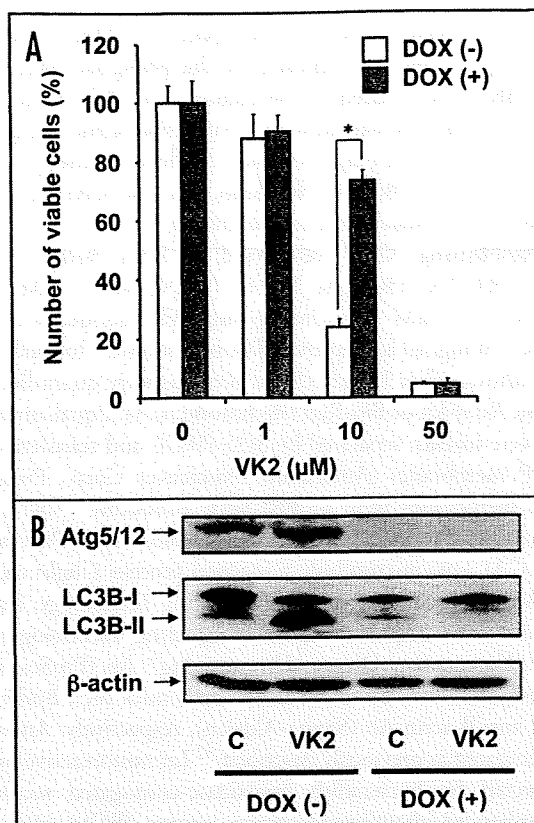
—190—
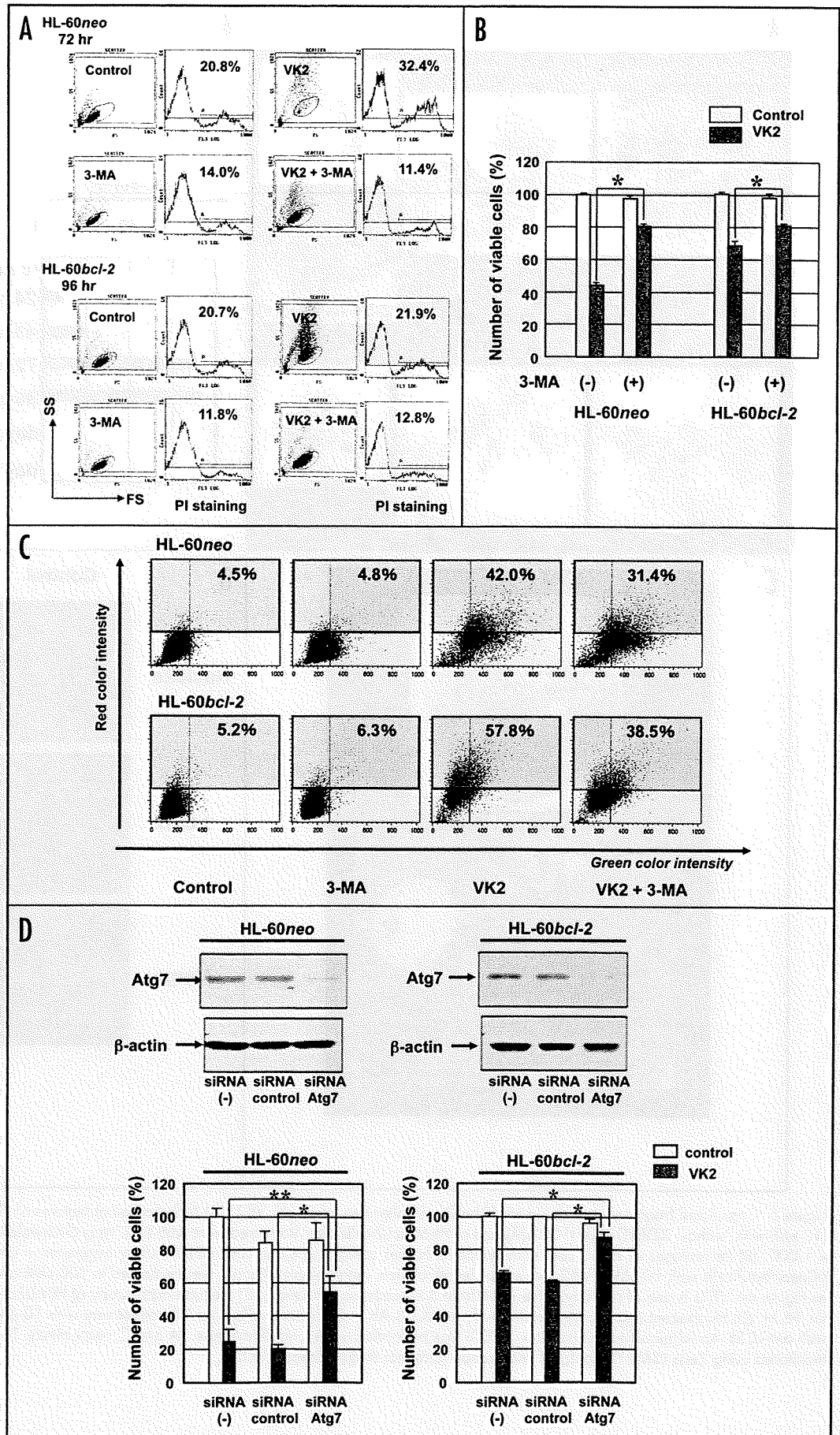
Figure 7. Effects of inhibition of VK2-inducing autophagy in a Atg5-/- mouse embryonic fibroblast (MEF) cell line with the Atg5 Tet-off system. Tet-off Atg5 MEF cells were incubated with 10 ng/ml doxycycline hydrochloride (Dox) for 120 hrs, and thereafter cultured in the presence or absence of 1 to 50 μM of VK2 for 72 hrs. (A) Cell growth inhibition in response to VK2 was assessed using WST assay kit. (B) MEF cells treated with or without Dox were cultured in the presence or absence of 10 μM of VK2 for 72 hr. Then, cellular proteins were separated by 11.25% SDS-PAGE and immunoblotted with either anti-Atg5, anti-LC3B, or anti-β-actin Abs.

autophagic processes can be simultaneously induced by VK2 (Figs. 2 and 3).[39,40] Therefore, cell death induced by cytotoxic reagents cannot be simply characterized in stereotyped manner such as type I PCD versus type II PCD.

Although autophagy became evident in HL-60bcl-2 cells, previous reports have demonstrated that Bcl-2 negatively regulates induction of autophagy. Bcl-2 localized on endoplasmic reticulum was reported to interact with Beclin 1 and to inhibit Beclin 1-dependent autophagy.[27] This anti-autophagy function of Bcl-2 was suggested to help maintain autophagy at the levels that are compatible with cell survival, rather than cell death.[27] In addition, downregulation of Bcl-2 by the conditional expression of the full length bcl-2 antisense message was reported to induce autophagic cell death in HL-60 cells,[26] and Bcl-2/Bcl-X$_L$ antagonist HA14-1 also induces autophagy and apoptosis in L1210 murine leukemia cells,[45] suggesting anti-autophagic function of Bcl-2. In our data, comparing autophagy induction between HL-60neo and HL-60bcl-2 by the formation of punctuated LC3B, autophagy was rather enhanced in HL-60neo cells within 72 hrs of exposure to VK2 (Fig. 3B). Delayed induction of autophagy in HL-60bcl-2 as assessed by conversion of LC3B type I to type II was also observed (Fig. 3D). These data agree with previous reports that Bcl-2 has a negative effect on the induction

of autophagy. However, since bcl-2 knockout mice are viable with almost intact bone marrow functions,[46] other regulatory pathway(s) might be involved for autophagy, especially when the cells are exposed to cytotoxic reagents. It has been reported that intracellular calcium mediates the induction of autophagy in a Bcl-2 regulated fashion.[47] These findings raise the question as to how a cell decides to undergo either apoptosis or autophagy in response to calcium signals.

It was intriguing that some morphologic features of the same death pathway differed between HL-60neo and HL-60bcl-2 cells. As shown in Figure 5A and B, nuclear fragments were capsulated in HL-60bcl-2 cells but not in HL60neo cells. Longer exposure to VK2 resulted in disappearance of this "sunny side-up" feature which seems to detect an early phase of apoptosis. These encapsulated nuclear fragments should be designated as "apoptotic bodies" as in previous reports.[48] The formation of "sunny side-up" may be only detectable under conditions for autophagy inductions along with a higher threshold for apoptosis such as overexpression of anti-apoptotic Bcl-2 proteins or in the presence of a caspase-3 inhibitor. However, we could not prove the macroautophagy formation of fragmented nuclei by LC3B fluorescence immunocytostaining (Fig. 5D) Biological significance of this distinct phenomenon remains to be cleared.

Although "autophagic cell death" has recently been clearly demonstrated in salivary gland cells during development of Drosophila,[49] the concept of autophagy as type II PCD is still controversial, especially the cell death induced by anti-cancer reagents.[20-22] In the presence of 3-MA, an inhibitor of type III PI3K, VK2-induced cell death was significantly suppressed not only in HL-60bcl-2 but also in HL-60neo cells (Fig. 6A–C). This suggests that the VK2-induced autophagy induces cell death. However, 3-MA is not a specific inhibitor for autophagy and it may interact with other signaling pathways for cell death.[22,37] Knockdown of Atg7 with siRNA prevented VK2-induced cell death (Fig. 6D). Tet-off Atg5 MEF system also demonstrated an attenuation of VK2-induced cell growth inhibition along with inhibition of autophagy (Fig. 7). Therefore, the enhanced autophagy in response to VK2 is correlated with induction for cell death in our system. These lines of evidence strongly suggest "autophagic cell death" or "autophagy medicated cell death" in leukemia cells. However, the executor(s) for induction of cell death still remains to be cleared. Yu Li et al., reported that caspase inhibition leading to cell death by means of autophagy involves accumulation of reactive oxygen species (ROS), membrane lipid oxidation, and loss of plasma membrane integrity in L929 cells.[50] The accumulation of abnormal ROS was caused by the selective autophagic degradation of the catalase, which is the major enzymatic ROS scavenger.[50] The accumulation of ROS following degradation of catalase might be one of the executors of autophagic cell death when caspases are inhibited. However, as shown in Figures 1A and 3D, catalase expression was not different between HL-60neo and HL-60bcl-2 cells, and no significant change of catalase expression during 96 hr exposure to VK2. Therefore, our observation cannot be explained by degradation of catalase. In fat body cells and wing discs of Drosophila, overexpression of Atg1 itself was sufficient to induce autophagy along with apoptosis in a caspase-dependent manner.[40] This suggests that autophagy represents an alternative induction of apoptosis rather than a distinct form of cell death. In contrast, autophagy is activated by apoptotic signaling in sympathetic neurons.[39] In this system, the same apoptotic signal induces

–191–

mitochondrial dysfunction and also activates autophagy. Once it was activated, autophagy was suggested to mediate caspase-independent neuronal death.[39] It is noteworthy that knockdown of Atg7 using siRNA as well as 3-MA treatment showed attenuation of growth inhibition by VK2 in HL-60*neo* cells (Fig. 6D). Since apoptotic cell death should be dominant in HL-60*neo* cells, autophagy may function as an alternative inducer for apoptosis. This may be further supported by the distinct morphologic change in some but not all HL-60*bcl-2* cells after longer exposure to VK2, which showed apoptotic bodies with "sunny side-up" feature (Fig. 4A and B).

Qu X et al., demonstrated that autophagy contributes to the clearance of dead cell by a mechanism that likely involves the generation of energy-dependent engulfment signals.[51] This suggests an extended role for autophagy in the disposal of dead cells by a phagocytic system in vivo. Although this novel function of autophagy for PCD was demonstrated in ES cells during embryonic development, it may also extend to cancer cells. Autophagy induction in response to VK2 may explain the selective clearance of a leukemic clone via the phagocytic system in vivo.[2,6,11] Autophagy induction by VK2 shown in this study may give us novel therapeutic tools in the treatment of leukemia.

Materials and Methods

Cell lines and reagents. HL-60 cells obtained from the American Type Culture Collection (Rockville, MD) were maintained in continuous culture in RPMI 1640 medium (GIBCO, Grand Island, NY) supplemented with 10% FCS (Hyclone, Logan, UT), 2 mM L-glutamine, penicillin (50 U/ml), and streptomycin (100 μg/ml). A clone stably transfected with the human *bcl-2* gene, HL-60*bcl-2*, was established by electroporation using a recombinant pdDNA3-plasmid-containing the human *bcl-2a* gene.[26] HL-60*neo* is a control cell line transfected with pdDNA3-plasmid alone.[26] VK2 (menaquinon-4) was supplied by Eisai Co., Ltd. (Tokyo, Japan). E-64-d and Pepstatin A, which are inhibitors for lysosomal proteases, were purchased from BIOMOL International L.P. (Plymouth Meeting, PA). Z-DEVD-FMK for a caspase-3 inhibitor was purchased from R & D Systems Inc. (Minneapolis, MN).

Assessment of viable cell count. HL-60 cells treated with or without VK2 were stained with a solution containing 1% (v/v) propidium iodide (PI) (Sigma-Aldrich, St. Louis, MO) for 30 min at 4°C. First, the gating area of cytogram for detecting viable HL-60 cells was established according to both the PI staining-negative area (indicating viable cells) and the forward- and side- scatter intensities.[2] Then the cell cultures were pipetted gently to obtain uniform cell suspension, and were introduced to a flow cytometer. The number of cells in gating area for viable HL-60 cells was assessed for 60 sec. The number relative to the cells treated with control medium revealed to be well-correlated with the results obtained from a WST Cell Counting Kit (Dojin East, Tokyo, Japan), with absorption measurements at 450 nm.[2] In some experiments viable cell counts were assessed by trypan blue dye exclusion.

Quantitative detection of acid vesicular organelles (AVOs) with acridine orange staining. Autophagy is the process of sequestrating cytoplasmic proteins and organelles into the lysosomal component and characterized by development of AVOs. To detect and quantify AVOs in VK2-treated cells, we performed vital staining with acridine orange (Polysciences, Warrington, PA) as described previously.[29,30]

To inhibit autophagy 2 mM 3-methyladenine (3-MA) (Polysciences Inc, Warrington, PA), an inhibitor of the phosphatidylinositol 3-kinase (PI3K),[31] was added to the cultures for 72 hr with/without VK2. HL-60 cells were stained with 1.0 μg/ml acridine orange for 15 min at room temperature and processed for flow cytometry using the FACScan Cytometer (Becton Dickinson, San Jose, CA) and analyzed with CellQuest software (Becton Dickinson).

Immunoblotting. Cells were lysed in Lysis Buffer (10 mM Tris-HCL PH 7.8, 150 mM NaCl, 1% NP-40, 1 mM EDTA, 10% glycerol, 1 mM phenylmethylsulfonyl fluoride, 0.15 U/ml aportinine, 10 mg/ml leupeptine, 100 mM sodium fluoride, 2 mM sodium orthovanadate), and cellular proteins were quantified using the Protein Assay kit of Bio-Rad (Richmond, CA). Equal amounts of proteins were loaded, separated by SDS-PAGE and transferred onto Hybond-P membranes (Amersham Biosciences Corp., Piscataway, NJ). The membranes were probed with antibodies (Abs) such as anti-human Bcl-2 monoclonal (m) Ab (BD Biosciences Pharmingen, San Jose, CA), anti-microtubule-associated protein 1 light chain 3B (LC3B) Ab, anti-caspase-3 Ab (Cell Signaling Technology, Danvers, MA), anti-cleaved caspase-3 Ab (Cell Signaling Technology), anti-Atg5 Ab (Abgent, San Diego, CA), anti-Atg7 Ab (ProSci, Poway, CA), anti-human catalase rabbit mAb (Epitomics Inc., Burlingame, CA), and anti-β-actin Ab (Sigma-Aldrich), respectively. Anti-LC3B Ab was generated as previously described.[32] Immunoreactive proteins were detected by horseradish peroxidase-conjugated second Ab and an enhanced chemiluminescence reagent (ECL) (Amersham Biosciences Corp.).[3]

Assessment of apoptosis. Apoptosis was detected by morphology, flow cytometry using Annexin V-florescein isothiocyanate (FITC) apoptosis detection kit I (BD Biosciences, San Diego, CA), and by immunoblotting with either anti-caspase-3 or anti-cleaved caspase-3 Abs as described above. For flow cytometry, HL-60 cells treated with or without VK2 were washed twice with ice cold phosphate-buffered saline and then resuspended in 1 X binding buffer (1 x 10^6 cells/ml). 100 μl of cell suspension (1 x 10^5 cells) was then transferred to a 5 ml tube, and 5 μl of Annexin V-PE and 5 μl of 7-amino-actinomycin were added. After 15 min of incubation at room temperature in the dark, 400 μl of 1 X binding buffer was added and the tubes were analyzed in a FACScan instrument with CellQuest software (Becton Dickinson). For morphologic assessment for apoptosis, the cell suspension was sedimented in a Shandon Cytospin II (Shandon, Pittsburgh, PA), and preparations were stained with May-Grünwald-Giemsa and with 4'-6-diamidino-2-phenylindole (DAPI, Vector laboratories, Inc., Burlingame, CA).

Measurement of mitochondrial membrane potential. Mitochondrial membrane potential was measured with tetramethyl rhodamine ethyl ester perchlorate (TMRE: Molecular Probe Inc., Eugene, OR) using flow cytometry as described previously.[30] Cells were incubated with 150 nM TMRE at 37°C for 20 min in the dark and analyzed by FACScan using CellQuest software. The fluorescent dye TMRE is accumulated by mitochondria as a result of the mitochondrial membrane potential. Shift to the left in the emission spectrum indicates the depolarization of mitochondrial membrane potential in the apoptotic cells.

Electron microscopy. HL-60 cells were treated with/without VK2 and then fixed with a solution containing 3% glutaraldehyde plus 2% paraformaldehyde in 0.1 M cacodylate buffer (pH 7.3) for

1 hr. The samples were further post-fixed in 1% OsO_4 in the same buffer for 1 hr, and subject to the electron microscopic analysis using an electron microscope H-7000 (Hitachi, Tokyo, Japan) as described previously.[30] Representative areas were chosen for ultra-thin sectioning and viewed with an electron microscope.

Fluorescent immunocytostaining. Cells were fixed on glass slide by Shandon Cytospin II followed by further fixation with 4% paraformaldehyde for 20 min. After fixation, the cells on the slides were incubated with anti-LC3B Ab (1:5,000 dilution) in 0.5% Triton X-100-phosphate-buffered saline (PBS) overnight at 4°C. The slides were then washed with PBS and incubated with Alexa Fluor 488-labeled secondary goat anti-rabbit Ab (1:200 dilution) for 1 hr at room temperature. The slides were mounted with DAPI and monitored under an Axioskop 40 (Carl Zeiss MicroImaging, Inc., Thornwood, NY) or LSM 510 (Carl Zeiss MicroImaging).

Small interfering RNA (siRNA) experiments. siRNA oligonucleotides for human Atg7 (accession # NM-006395, catalog # L-020112), and siCONTROL non-targeting siRNA (catalog # D-001220) were purchased from GE Healthcare UK Ltd. (Buckinghamshire, England), and resuspended in RNase-free H_2O at 20 µM. HL-60*bcl-2* cells were washed twice in serum-free media and resuspended to 1×10^7 cells per 500 µl of cold, serum-free OPTI-MEM (GIBCO), and transferred to pre-chilled 0.4 cm-gap electroporation curettes (Bio-Rad). Cells were mixed with/without siRNA at 20 nM (final concentration) on ice for 5 min, thereafter, cells were pulsed once at 250 mV, 960 µF by using a Bio-Rad electroporator. The cell suspensions were then transferred to the incubator in 5% CO_2 at 37°C. Five hr after electroporation, the same volume of RPMI 1640 medium containing 20% FBS was added. Forty-eight hr after electroporation, protein knockdown was determined by immunoblotting, and the cells were treated with the indicated concentration of VK2 for 72 to 96 hr, and viable cells were assessed as previously described.

Tet-off system with an Atg5$^{-/-}$ mouse embryonic fibroblasts (MEFs). The Atg5 Tet-off MEF cell line was a kind gift from Dr Noboru Mizushima (Tokyo Medical and Dental University School of Health Science, Tokyo, Japan).[33] Atg 5 expression can be completely suppressed when this cell line is cultured in the presence of doxycycline. The culture condition is precisely described in elsewhere.[33]

Statistics. All data are given as the mean ± SD. Statistical analysis was performed by using Mann-Whitney's U test (two-tailed). The criterion for statistical significance was taken as p < 0.05.

References

1. Lamson DW, Plaza SM. The anticancer effects of vitamin K. Altern Med Rev 2003; 8:303-18.
2. Yaguchi M, Miyazawa K, Katagiri T, Nishimaki J, Kizaki M, Tohyama K, Toyama K. Vitamin K2 and its derivatives induce apoptosis in leukemia cells and enhance of all-*trans* retinoic acid. Leukemia 1997; 11:779-87.
3. Yokoyama T, Miyazawa K, Yoshida T, Ohyashiki K. Combination of vitamin K2 plus imatinib mesylate enhances induction of apoptosis in small cell lung cancer cell lines. Int J Oncol 2005; 26:33-40.
4. Wang Z, Wang M, Finn F, Carr BI. The growth inhibitory effects of vitamins K and their actions on gene expression. Hepatology 1995; 22:876-82.
5. Otsuka M, Kato N, Shao RX, Hoshida Y, Ijichi H, Koike Y, Taniguchi H, Moriyama M, Shiratori Y, Kawabe T, Omata M. Vitamin K2 inhibits the growth and invasiveness of hepatocellular carcinoma cells via protein kinase A activation. Hepatology 2004; 40:243-51.
6. Miyazawa K, Aizawa S. Vitamin K2 improves the hematopoietic supportive functions of bone marrow stromal cells in vitro: a possible mechanism of improvement of cytopenia for refractory anemia in response to vitamin K2 therapy. Stem Cells Dev 2004; 5:449-51.
7. Miyazawa K, Nishimaki J, Ohyashiki K, Enomoto S, Kuriya S, Fukuda R, Hotta T, Teramura M, Mizoguchi H, Uchiyama T, Omine M. Vitamin K2 therapy for myelodysplastic syndrome (MDS) and post-MDS acute myeloid leukemia: Information through a questionnaire survey of multi-center pilot studies in Japan. Leukemia 2000; 14:1156-7.
8. Yaguchi M, Miyazawa K, Otawa M, Ito Y, Kawanishi Y, Toyama K. Vitamin K2 therapy for a patient with myelodysplastic syndrome. Leukemia 1999; 13:144-5.
9. Habu D, Shiomi S, Tamori A, Takeda T, Tanaka T, Kubo S, Nishiguchi S. Role of vitamin K_2 in the development of hepatocellular carcinoma in women with viral cirrhosis of the liver. *JAMA* 2004; 292:358-61.
10. Mizuta T, Ozaki I, Eguchi Y, Yasutake T, Kawazoe S, Fujimoto K, Yamamoto K. The effect of menatetrenone, a vitamin K_2 analog, on disease recurrence and survival in patients with hepatocellular carcinoma after curative treatment: a pilot study. Cancer 2006; 106:867-72.
11. Yaguchi M, Miyazawa K, Otawa M, Katagiri T, Nishimaki J, Uchida Y, Iwase O, Gotoh A, Kawanishi Y, Toyama K. Vitamin K2 selectively induces apoptosis of blastic cells in myelodysplastic syndrome: Flow cytometric detection of apoptotic cells using APO2.7 monoclonal antibody. Leukemia 1998; 12:1392-7.
12. Miyazawa K, Yaguchi M, Funato K, Gotoh A, Kawanishi Y, Nishizawa Y, Yuo A, Ohyashiki K. Apoptosis/differentiation-inducing effects of vitamin K2 on HL-60 cells: dichotomous nature of vitamin K2 in leukemia cells. Leukemia 2001; 15:1111-7.
13. Nishimaki J, Miyazawa K, Yaguchi M, Katagiri T, Kawanishi Y, Toyama K, Ohyashiki K, Hashimoto S, Nakaya K, Takiguchi T. Vitamin K2 induces apoptosis of a novel cell line established from a patient with myelodysplastic syndrome in blastic transformation. Leukemia 1999; 9:1399-405.
14. Matsumoto K, Okano J, Nagahara T, Murawaki Y. Apoptosis of liver cancer cells by vitamin K2 and enhancement by MEK inhibition. Int J Oncol 2006; 29:1501-8.
15. Kanamori T, Shimizu M, Okuno M, Matsushima-Nishiwaki R, Tsurumi H, Kojima S, Moriwaki H. Synergistic growth inhibition by acyclic retinoid and vitamin K2 in human hepatocellular carcinoma cells. Cancer Sci 2007; 98:431-7.
16. Martelli AM, Zweyer M, Ochs RL, Tazzari PL, Tabellini G, Narducci P, Bortul R. Nuclear apoptotic changes: an overview. J Cell Biochem 2001; 82:634-46.
17. Green DR, Reed JC. Mitochondria and apoptosis. Science 1998; 281:1309-12.
18. Reed JC. Apoptosis-targeted therapies for cancer. Cancer Cell 2003; 3:17-22.
19. Clarke P. Developmental cell death: morphological diversity and multiple mechanisms. Anat Embryol (Berl) 1990; 181:195-213.
20. Bursch W, Ellinger A, Gerner C, Frohwein U, Schulte-Hermann R. Programmed cell death (PCD). Apoptosis, autophagic PCD, or others? Ann N Y Acad Sci 2000; 926:1-12.
21. Kondo Y, Kanzawa T, Sawaya R, Kondo S. Role of autophagy in cancer development and response to therapy. Nat Rev Cancer 2005; 5:726-34.
22. Levine B, Yuan J. Autophagy in cell death: an innocent convict? J Clin Invest 2005; 115:2679-88.
23. Klionsky D J, Emr SD. Autophagy as a regulated pathway of cellular degradation. Science 2000; 290:1717-21.
24. Yoshimori T. Autophagy: a regulated bulk degradation process inside cells. Biochem Biophysical Research Communications 2004; 313:453-8.
25. Ohsumi Y. Molecular dissection of autophagy: two ubiquitin-like systems. Nat Rev Mol Cell Biol 2001; 3:211-6.
26. Saeki K, Yuo A, Okuma E, Yazaki Y, Susin SA, Kroemer G, Takaku F. Bcl-2 downregulation causes autophagy in a caspase-independent manner in human leukemic HL60 cells. Cell Death Differ 2000; 12:1263-9.
27. Pattingre S, Tassa A, Qu X, Garuti R, Liang XH, Mizushima N, Packer M, Schneider MD, Levine B. Bcl-2 antiapoptotic proteins inhibit Beclin 1-dependent autophagy. Cell 2005; 122:927-39.
28. Pattingre S, Levine B. Bcl-2 inhibition of autophagy: A new route to cancer? Cancer Res 2006; 66:2885-8.
29. Paglin S, Hollister T, Delohery T, Hackett N, McMahill M, Sphicas E, Domingo D, Yahalom J. A novel response of cancer cells to radiation involves autophagy and formation of acidic vesicles. Cancer Res 2001; 61:439-44.
30. Kanzawa T, Kondo Y, Ito H, Kondo S, Germano I. Induction of autophagic cell death in malignant glioma cells by arsenic trioxide. Cancer Res 2003; 63:2103-8.
31. Seglen PO, Gordon PB. 3-Methyladenine: specific inhibitor of autophagic/lysosomal protein degradation in isolated rat hepatocytes. Proc Natl Acad Sci USA 1982; 79:1889-92.
32. Aoki H, Takada Y, Kondo S, Sawaya R, Aggarwal BB, Kondo Y. Evidence that curcumin suppresses the growth of malignant gliomas in vitro and in vivo through induction of autophagy: role of Akt and extracellular signal-regulated kinase signaling pathways. Mol Pharmacol 2007; 72:29-39.
33. Hosokawa N, Hara Y, Mizushima N. Genaration of cell lines with teracycline-regulated autophagy and a role for autophagy in controlling cell size. FEBS Letters 2006; 580:2623-9.

34. Kabeya Y, Mizushima N, Ueno T, Yamamoto A, Kirisako T, Noda T, Kominami E, Ohsumi Y, Yoshimori T. LC3, a mammalian homologue of yeast Apg8p, is localized in autophagosome membranes after processing. EMBO J 2000: 19:5720-8.

35. Mizushima N. Methods for monitoring autophagy. Int J Biochem Cell Biol 2004; 36:2491-502.

36. Mizushima N, Yoshimori T. How to interpret LC3 immunoblotting. Autophagy 2007; 3:1-4.

37. Klionsky DJ, Abeliovich H, Agostinis P, et al. Guidelines for the use and interpretation of assays for monitoring autophagy in higher eukaryotes. Autophagy 2008; 4:151-75.

38. Tanida I, Minematsu-Ikeguchi N, Ueno T, Kominami E. Lysosomal turnover, but not a cellular level, of endogenous LC3 is a marker for autophagy. Autophagy 2005; 1:84-91.

39. Xue L, Fletcher GC, Tolkovsky AM. Autophagy is activated by apoptotic signalling in sympathetic neurons: an alternative mechanism of death execution. Mol Cell Neurosci 1999; 14:180-98.

40. Scott RC, Juhász G, Neufeld TP. Direct induction of autophagy by Atg1 inhibits cell growth and induces apoptotic cell death. Curr Biol 2007; 17:1-11.

41. Kanzawa T, Germano IM, Komata T, Ito H, Kondo Y, Kondo S. Role of autophagy in temozolomide-induced cytotoxicity for malignant glioma cells. Cell Death Differ 2004; 11:448-57.

42. Shao Y, Gao Z, Marks PA, Jiang X. Apoptotic and autophagic cell death induced by histone deacetylase inhibitors. Proc Natl Acad Sci USA 2004; 101:18030-5.

43. Yu L, Alva A, Su H, Dutt P, Freundt E, Welsh S, Baehrecke EH, Lenardo MJ. Regulation of an ATG7-beclin 1 program of autophagic cell death by caspase-8. Science 2004; 304:1500-2.

44. Shimizu S, Kanaseki T, Mizushima N, Mizuta T, Arakawa-Kobayashi S, Thompson CB, Tsujimoto Y. Role of Bcl-2 family proteins in a non-apoptotic programmed cell death dependent on autophagy genes. Nat Cell Biol 2004; 6:1221-8.

45. Kessel D, Reiners JJ Jr. Initiation of apoptosis and autophagy by the Bcl-2 antagonist HA14-1. Cancer Lett 2007; 249:294-9.

46. Nakayama K, Nakayama K, Negishi I, Kuida K, Sawa H, Loh DY. Targeted disruption of Bcl-2 alpha beta in mice: occurrence of gray hair, polycystic kidney disease, and lymphocytopenia. Proc Natl Acad Sci USA 1994; 91:3700-4.

47. Hoyer-Hansen M, Bastholm L, Szyniarowski P, Campanella M, Szabadkai G, Farkas T, Bianchi K, Fehrenbacher N, Elling F, Rizzuto R, Mathiasen IS, Jaattela M. Control of macroautophagy by calcium, calmodulin-dependent kinase kinase-beta, and Bcl-2. Mol Cell 2007; 25:193-205.

48. Martelli AM, Zweyer M, Ochs RL. Nuclear apoptotic changes: an overview. J Cellular Biochemistry 2001; 82:634-46.

49. Berry DL, Baehrecke EH. Growth arrest and autophagy are required for salivary gland cell degradation in Drosophila Cell 131:1137-48.

50. Yu L, Wan F, Dutta S, Welsh S, Liu Z, Freundt E, Baehrecke EH, Lenardo M. Autophagic programmed cell death by selective catalase degradation. Proc Natl Acad Sci USA 2006; 103:4952-7.

51. Qu X, Zou Z, Sun Q, Luby-Phelps K, Cheng P, Hogan RN, Gilpin C, Levine B. Autophagy gene-dependent clearance of apoptotic cells during embryonic development. Cell 2007; 128:931-46.

KTZ-1288

AML1 mutations induced MDS and MDS/AML in a mouse BMT model

Naoko Watanabe-Okochi,[1] Jiro Kitaura,[1] Ryoichi Ono,[1] Hironori Harada,[2] Yuka Harada,[3] Yukiko Komeno,[1] Hideaki Nakajima,[1] Tetsuya Nosaka,[1] Toshiya Inaba,[4] and Toshio Kitamura[1]

[1]Division of Cellular Therapy, Advanced Clinical Research Center, The Institute of Medical Science, The University of Tokyo, Tokyo; [2]Department of Hematology and Oncology, Research Institute for Radiation Biology and Medicine, Hiroshima University, Hiroshima; [3]International Radiation Information Center, Research Institute for Radiation Biology and Medicine, Hiroshima University, Hiroshima; and [4]Department of Molecular Oncology, Research Institute for Radiation Biology and Medicine, Hiroshima University, Hiroshima, Japan

Myelodysplastic syndrome (MDS) is a hematopoietic stem-cell disorder characterized by trilineage dysplasia and susceptibility to acute myelogenous leukemia (AML). Analysis of molecular basis of MDS has been hampered by the heterogeneity of the disease. Recently, mutations of the transcription factor AML1/RUNX1 have been identified in 15% to 40% of MDS–refractory anemia with excess of blasts (RAEB) and MDS/AML. We performed mouse bone marrow transplantation (BMT) using bone marrow cells transduced with the *AML1* mutants. Most mice developed MDS and MDS/AML-like symptoms within 4 to 13 months after BMT. Interestingly, among integration sites identified, Evi1 seemed to collaborate with an *AML1* mutant harboring a point mutation in the Runt homology domain (D171N) to induce MDS/AML with an identical phenotype characterized by marked hepatosplenomegaly, myeloid dysplasia, leukocytosis, and biphenotypic surface markers. Collaboration between AML1-D171N and *Evi1* was confirmed by a BMT model where coexpression of AML1-D171N and *Evi1* induced acute leukemia of the same phenotype with much shorter latencies. On the other hand, a C-terminal truncated *AML1* mutant (S291fsX300) induced pancytopenia with erythroid dysplasia in transplanted mice, followed by progression to MDS-RAEB or MDS/AML. Thus, we have developed a useful mouse model of MDS/AML that should help in the understanding of the molecular basis of MDS and the progression of MDS to overt leukemia. (Blood. 2008;111:4297-4308)

© 2008 by The American Society of Hematology

Introduction

Myelodysplastic syndromes (MDS) are a heterogeneous group of clonal stem-cell disorders characterized by ineffective hematopoiesis and susceptibility to leukemic transformation (MDS/acute myelogenous leukemia [AML]). Progression from MDS-refractory anemia with excess blasts (MDS-RAEB) to AML is frequently observed in the clinical course, which is thought to result from serial acquisition of cytogenetic abnormalities.[1-5] According to the 2-hit model of leukemogenesis, one class of mutations (class I), including FLT3-ITD, N-Ras, or K-Ras mutations, confers on cells a proliferative advantage; a second class of mutations (class II), including AML1/ETO, PML/RARα, or MLL-related fusion genes, interferes with hematopoietic differentiation.[6] Indeed, it has been reported that a combination of class I and II mutations such as FLT3-ITD plus AML1-ETO or MLL-SEPT6 induced AML in a mouse bone marrow transplantation (BMT) model, while either class I or II mutations alone led to, if anything, myeloproliferative disorders (MPDs), not leukemia.[6-13] On the other hand, the precise molecular mechanism underlying development of MDS and MDS/AML remains elusive partly because there are only a few mouse models for MDS and MDS/AML available. So far, 2 distinct models of MDS have been reported: *Evi1* induced MDS-like symptoms in a mouse BMT model in which the mice succumbed to fatal peripheral cytopenia,[14] while NUP98-HOXD13 transgenic mice developed MDS and died of either various types of acute leukemia or severe anemia and leukocytopenia.[15] In the present study, we generated a mouse BMT model of MDS-RAEB and MDS/AML induced by *AML1* mutants frequently found in patients with MDS and MDS/AML. Interestingly, the phenotypes of these mice very much resemble those of the human diseases.

The *AML1* gene is located on chromosome 21q22 and is the most frequent target for chromosomal translocation in leukemia. Analysis of AML1-deficient mice has shown that *AML1* is indispensable for the establishment of definitive hematopoiesis.[16-18] As accumulated studies have demonstrated, heterozygous germline mutations in the *AML1* gene caused familial platelet disorder with predisposition to AML (FPD/AML),[19,20] and sporadic point mutations were frequently found in the development of leukemia: 21% of AML M0, 15.0% to 15.9% of MDS-RAEB and MDS/AML, and 46% of radiation-associated MDS.[21-29] The vast majority of AML1 mutations were located in the Runt homology domain (RHD), which mediated its ability to bind to DNA and core-binding factor β (CBFβ). To confirm the involvement of *AML1* mutations in hematopoietic disorders, we selected 2 types of *AML1* mutants found in patients with MDS/AML: one with a point mutation in RHD (AML1-D171N), and the other with C-terminal truncation caused by a frame-shift (AML1-S291fsX300). After transplantation using bone marrow cells infected with retrovirus vectors harboring *AML1* mutants, most of the mice that received transplants died of MDS-RAEB and MDS/AML. Long-term analysis demonstrated that the phenotype of the mice that underwent

transplantation depended on the kind of *AML1* mutants used in this study and on the integration sites of retroviruses. Considering the recent reports of the effects of retrovirus integration sites on biological results,[30-38] identification of integration sites may lead to the discovery of the genes involved in the induction of MDS/AML in concert with *AML1* mutants. Intriguingly, the enhanced expression of Evi1 by retrovirus integration seemed to collaborate with AML1-D171N to induce MDS/AML with the same phenotype. Moreover, we confirmed that combination of AML1-D171N and *Evi1* induced AML of the same phenotype with shorter latencies in the mouse BMT model. This model will allow valuable insight into the molecular pathogenesis of MDS and MDS/AML.

Methods

Vector construction

We used 2 *AML1* mutants, D171N or S291fsX300, identified from case no. 5 or 27, respectively, among patients with MDS/AML.[25,26] These mutants are hereafter referred to as AML1-D171N and AML1-S291fs. AML1 wild-type (WT; AML1b), AML1-D171N, or AML1-S291fs, which was fused with a FLAG epitope tag at the N-terminus, was inserted upstream of the IRES-EGFP cassette of pMYs-IG to generate pMYs-AML1 WT, D171N, or S291fs-IG, respectively. pMYs-mouse Evi1-IG were kindly provided by Dr T. Nakamura (The Cancer Institute, Tokyo, Japan).[38]

Transfection and retrovirus production

Plat-E[39] packaging cells maintained in Dulbecco modified Eagle medium (DMEM) supplemented with 10% fetal calf serum (FCS) were transfected with retroviral constructs by using FuGENE 6 (Roche Diagnostics, Mannheim, Germany) according to the manufacturer's recommendations. The medium was changed 1 day after the transfection, and retroviruses were harvested 48 hours after the transfection as previously described.[39,40] Titers of the retroviruses were assessed based on the number of neomycin-resistant colonies of the infected NIH3T3 cells (average: 10[7] infection U/mL) as described.[39]

Mouse BMT

Bone marrow mononuclear cells were isolated from the femurs and tibias of C57BL/6 (Ly-5.1) donor mice (9-12 weeks of age) 4 days after intraperitoneal administration of 150 mg/kg 5-fluorouracil (5-FU) and cultured overnight in α minimal essential medium (αMEM) supplemented with 20% FCS and 50 ng/mL of mouse stem cell factor (SCF), mouse FLT3 ligand (FL), human IL-6, and human thrombopoietin (TPO; R&D Systems, Minneapolis, MN). The prestimulated cells were infected for 60 hours with the retroviruses harboring pMYs-AML1 WT, D171N, or S291fs-IG, or an empty vector as a control, using 6-well dishes coated with RetroNectin (Takara Bio, Shiga, Japan) according to the manufacturer's recommendations. Then, 0.2 to 3.5 × 10^{6} of infected bone marrow cells (Ly-5.1) were injected through tail vein into C57BL/6 (Ly-5.2)–recipient mice (8-12 weeks of age) which had been administered a sublethal dose of 5.25 Gy or a lethal dose of 9.5 Gy total-body γ-irradiation ([135]Cs). For the lethally irradiated mice, a radioprotective dose of 2 × 10^{5} of bone marrow cells (Ly-5.2) was simultaneously injected. Probabilities of overall survival of the mice that received transplants were estimated using the Kaplan-Meier method. All animal studies were approved by the Animal Care Committee of the Institute of Medical Science, The University of Tokyo.

Analysis of the mice that underwent transplantation

Engraftment of bone marrow cells infected with retroviruses was confirmed by measuring the percentage of GFP+ and Ly-5.1+ cells in peripheral blood obtained every 1 to 2 months after the transplantation.

After the morbid mice were killed, their tissue samples, including peripheral blood (PB), bone marrow (BM), spleen, liver, and kidney, were analyzed. Circulating blood cells were counted by an analyzer. Morphology of the peripheral blood was evaluated by staining of air-dried smears with Hemacolor (Merck, Darmstadt, Germany). Tissues were fixed in 10% buffered formalin, embedded in paraffin, sectioned, and stained with hematoxylin and eosin (H&E). Cytospin preparations of bone marrow and spleen cells were also stained with Hemacolor. Percentage of blasts, myelocytes, neutrophils, monocytes, lymphocytes, and erythroblasts was estimated by examination of at least 200 cells. To assess whether the leukemic cells were transplantable, 2 × 10^{5} to 10[6] total BM cells including blasts were injected into the tail veins of sublethally irradiated mice. A total of 2 or 3 recipient mice were used for each serial transplantation.

Flow cytometric analysis

Red blood cells were lysed by using Ammonium Chloride Lysing Reagent (BD Biosciences, San Jose, CA) in PB or single-cell suspensions of bone marrow and spleen. Washed cells were incubated for 15 minutes at 4°C with 2.4G2 antibody for blocking and then stained for 20 minutes at 4°C with the following monoclonal phycoerythrin (PE)–conjugated antibodies: Ly-5.1, Gr-1, CD11b, B220, CD3, CD41, c-Kit, Sca-1, CD34, and Ter119. Flow cytometric analysis of the stained cells was performed with FACSCalibur flow (BD Biosciences) equipped with CellQuest software (BD Biosciences) and Flowjo software (Tree Star, San Carlos, CA).

Diagnosis

Diagnosis was made according to the Bethesda proposals for classification of nonlymphoid hematopoietic neoplasms in mice.[41]

Real-time RT-PCR

Total RNA was extracted from BM cells using Trizol (Invitrogen, Carlsbad, CA). cDNA was prepared with the Superscript II RT kit (Invitrogen). Real-time reverse transcription–polymerase chain reaction (RT-PCR) was performed using a LightCycler Workflow System (Roche Diagnostics). cDNA was amplified using a SYBR Premix EX Taq (TAKARA). Reaction was subject to one cycle of 95°C for 30 seconds, 45 cycles of PCR at 95°C for 5 seconds, 55°C for 10 seconds, and 72°C for 10 seconds. All samples were independently analyzed at least 3 times. The following primer pairs were used: 5'-CCAGATGTCACATGACAGTGGAAAGCACTA-3' (forward) and 5'-CCGGGTTGGCATGACTCATATTAACCATGG-3' (reverse) for Evi1; 5'-TACCTCAACCCCTGACAGCTATGG-3' (forward) and 5'-TCGGTTGGAGATATCAGAGTGCAG-3' (reverse) for MN1;[42] and 5'-GTTATCCCATCTGCATCAGCATCTGG-3' (forward) and 5'-GGTCCTCTTCACTCTTCATGAACAGC-3' (reverse) for MDS1/Evi1.[43] Relative gene expression levels were calculated using standard curves generated by serial dilutions of cDNA. Product quality was checked by melting curve analysis via LightCycler software (Roche Diagnostics). Expression levels were normalized by a control, the expression level of GAPDH mRNA.

Western blot analysis

To detect the expression of *AML1* WT, mutants, or *Evi1*, equal numbers of spleen cells were lysed, and Western blotting was performed as described with minor modifications.[13] Polyclonal rabbit anti-Evi1 antibody (a kind gift from Dr M. Kurokawa, Tokyo University, Tokyo, Japan), or a monoclonal mouse anti-Flag antibody (Sigma-Aldrich, St Louis, MO) was used for *Evi1* or *AML1*, respectively.

Southern blot analysis

Genomic DNA was extracted from BM or spleen cells. After enzymatic digestion of 10 μg DNA with *Eco*RI followed by electrophoretic separation, proviruses were probed with a GFP probe.

Bubble PCR

A total of 10 μg of genomic DNA extracted from BM or spleen cells was digested with *Eco*RI, and the fragments were ligated overnight at 16°C to a double-stranded bubble linker (5'-AATTGAAGGAGAGGACGCTGTCTG-
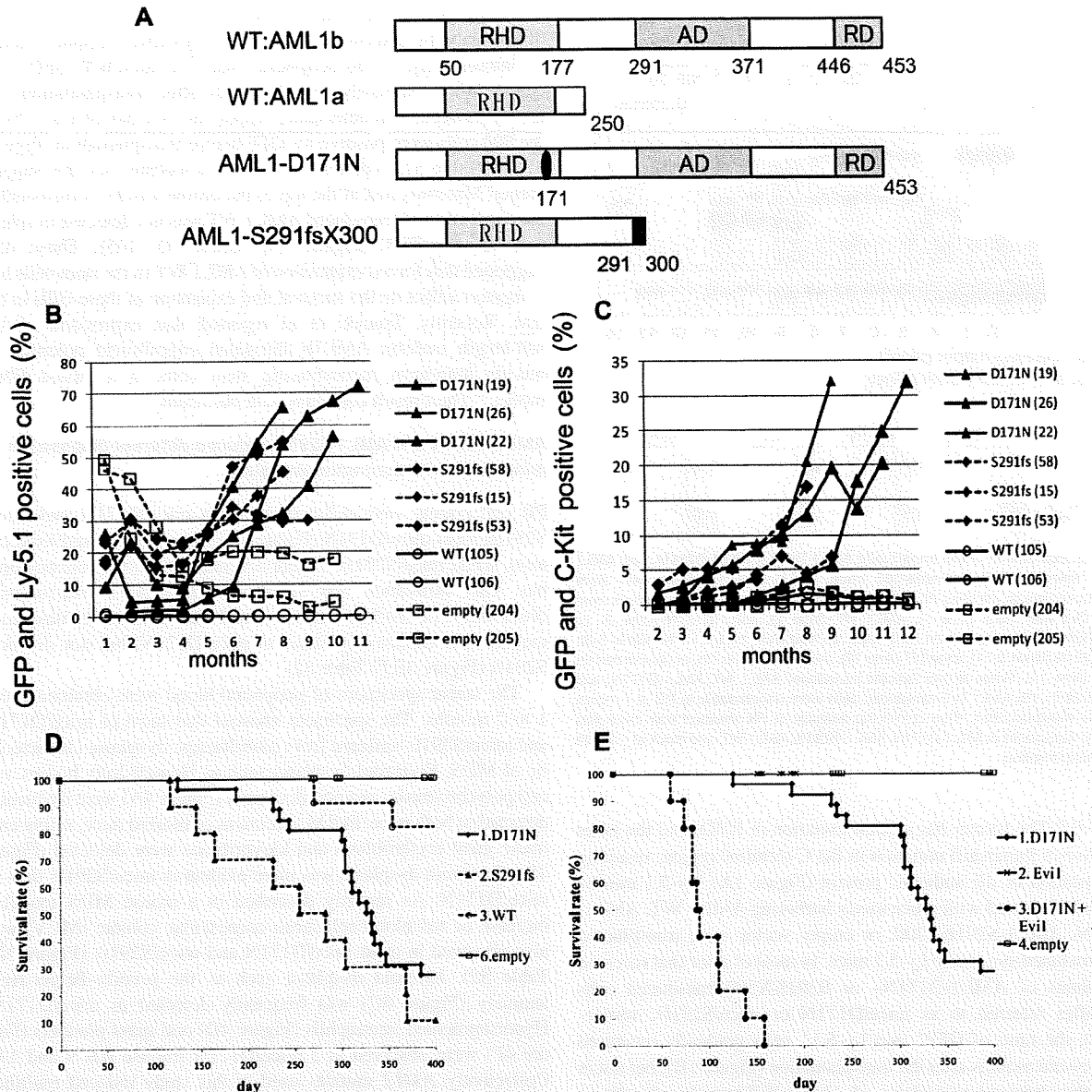
Figure 1. MDS and MDS/AML induced by *AML1* mutants derived from patients with MDS. (A) Schematics of *AML1* WT (AML1a and AML1b) and *AML1* mutants (D171N and S291fs). AD indicates transactivating domain; RD, repression domain. (B) Percentages of GFP/Ly-5.1 double-positive cells or (C) c-Kit$^+$ cells in PB. PB was obtained from the tail vein every month after the transplantation. Numbers in parenthesis indicate mouse IDs. (D) Kaplan-Meier analysis for the survival of mice that received transplants of *AML1* mutant-transduced BM cells. Average survival days of AML1-D171N (340.6 days) were compared with AML1-S291fs (263.6 days) using the log-rank test; *P* = .218. AML1 WT (n = 11), D171N (n = 26), S291fs (n = 10), mock (n = 16). (E) Evi1 synergized with AML1-D171N in inducing MDS/AML. D171N (n = 26; same as those in panel D), Evi1 (n = 8), D171N + Evi1 (n = 10), and mock (n = 16) transduced bone marrow cells were transplanted into mice.

TCGAAGGTAAGGAACGGACGAGAGAAGGGAGAG-3' and 5'-GACTC-TCCCTTCTCGAATCGTAACCGTTCGTACGAGAATCGCTGTCCTCTCC-TTC-3').[44] Next, PCR was performed on the ligation product using a linker-specific Vectorette primer (5'-CGAATCGTAACCGTTCGTACGAGAATCGCT-3')[44,45] and a long-terminal repeat (LTR)–specific primer (5'-CGAGCTCAATAAAA-GAGCCCACAACCCC-3') under the following conditions: one cycle of 95°C for 5 minutes, 10 cycles of 95°C for 30 seconds, and 67°C for 30 seconds and 72°C for 3 minutes, 10 cycles of 95°C for 30 seconds, and 67°C (this annealing temperature was reduced by 1°C each cycle) for 30 seconds and 72°C for 3 minutes, 15 cycles of 95°C for 30 seconds and 57°C for 30 seconds and 72°C for 3 minutes, and one cycle of 72°C for 90 seconds. Next, nested PCR was performed on 2 μL of PCR products using a linker-specific Vectorette primer and an LTR-specific primer (5'-ATAAAAGAGCCCACAACCCCTCACTCGG-3') under the following conditions: 1 cycle of 95°C for 5 minutes, 35 cycles of 95°C for 30 seconds and 60°C for 30 seconds and 72°C for 3 minutes, and 1 cycle of 72°C for 90 seconds.

The PCR product was electrophoresed using 1.0% agarose gel. Individual bands were excised and purified using PCR clear (Promega, Madison, WI) and were sequenced to identify the integration site of retrovirus. We confirmed inverse repeat sequence "GGGGGTCTTTCA" as a marker of junction between genomic DNA and retrovirus sequence.

Results

The ratio of *AML1* mutant-transduced cells gradually increased over several months after transplantation

To examine the effect of *AML1* mutants on the hematopoietic abnormality, we chose 2 distinct mutants, AML1-D171N and AML1-S291fsX300, which are found in patients with MDS/

A

IB: anti Flag (upper panel)
IB: anti tubulin (lower panel)

B
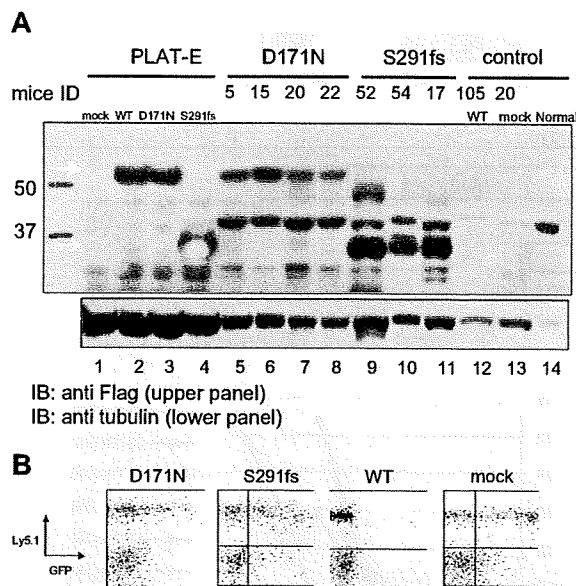
Figure 2. Expression of the transduced AML1-D171N, AML1-S291fs, and AML1 WT in spleen of the transplanted mice. (A) Lysates of spleen cells were immunoblotted with anti-Flag Ab. As a positive control, Plat-E packaging cells were transduced with mock (lane 1), AML1 WT (lane 2), AML1-D171N (lane 3), or AML1-S291fs (lane 4). Spleen cells were derived from mice/D171N (lanes 5-8), mice/S291fs (lanes 9-11), mice/WT (lane 12), mice/mock (lane 13), or control normal mouse (lane 14). White arrows indicate transduced AML1 WT, AML1-D171N, and AML1-S291fs. (B) AML1 WT-transduced cells were undetectable in PB at 1 month after the transplantation. Flow cytometric analysis of PB obtained from mice that received transplants of AML1-D171N, AML1-S291fs, AML1 WT, and mock at 1 month after transplantation.

AML.[25,26] The former has a point mutation in RHD, and the latter possesses a frameshift mutation in the C-terminal region, resulting in truncation of the authentic protein (Figure 1A). Ly-5.1 murine BM cells infected with retroviruses harboring AML1 WT, AML1-D171N, AML1-S291fsX300, or empty vector were transplanted into irradiated syngeneic Ly-5.2 mice. In most of mice that received transplants of AML1-D171N- or S291fsX300-transduced cells (hereafter referred to as mice/D171N or mice/S291fs, respectively), the ratio of GFP⁺ and Ly-5.1⁺ cells gradually increased over several months after the transplantation (Figure 1B), but not in mice that received transplants of AML1 WT-transduced cells or control retrovirus-infected cells (hereafter referred to as mice/WT or mice/mock, respectively). Gradual increase of c-kit⁺ cells in the PB was also observed in the mice that received transplants of AML1 mutant-transduced cells during the observation period (Figure 1C). Cells positive for c-kit and GFP—that is, c-kit⁺ cells transduced with AML1 mutants—were morphologically blasts with high nuclear-cytoplasmic ratios (data not shown). In fact, the percentage of blasts gradually increased in the PB of the mice that received transplants of AML1 mutant-transduced cells, especially the mice/D171N. Finally, most of mice/D171N or mice/S291fs became sick and died with latencies of 4 to 13 months after the transplantation, while mice/mock were healthy over the observation period (Figure 1D). Overall survival of mice/D171N was not significantly different from that of mice/S291fs ($P = .218$). Expression of the transduced AML1-D171N or AML1-S291fs in spleen cells was confirmed by Western blot analysis (Figure 2A). Two of the mice/WT died during the observation period. BM of the 2 mice was occupied with GFP/Ly5.1 double-negative cells. One of the mice/WT developed leukemia derived from recipient cells at

272 days after transplantation. The remaining one mouse/WT died of anemia with unknown reason at 355 days after transplantation.

Interestingly, in the peripheral blood of mice/WT, GFP⁺ cell counts were extremely low 1 month after transplantation and thereafter became undetectable, despite the fact that 14% to 27% of the BM cells were positive for GFP before transplantation (Figures 1B,2B; Table S1, available on the Blood website; see the Supplemental Materials link at the top of the online article). Consistently, the expression of transduced AML1 WT was not detected in spleen cells of mice/WT (Figure 2A; mouse ID: 105). These data suggested that forced expression of AML1 WT in the stem cells had a negative effect on the survival and expansion of these cells in the BM. Recently, Tsuzuki et al reported that expression of the full-length isoform AML1b abrogated engraftment potential of murine long-term reconstituting stem cells in a mouse BMT model.[46] Their result coincides with our result.

AML1-D171N and AML1-S291fs induced different diseases in mice that underwent transplantation

PB cell counts were different between mice/D171N and mice/S291fs; most mice/D171N (Figure 3A; lanes 1,2) showed leukocytosis, while mice/S291fs (Figure 3A; lane 3) showed leukocytopenia. This difference was significant ($P = .007$). Macroscopic observation of morbid mice revealed that severe hepatosplenomegaly was exclusively found in mice/D171N, but not in mice/S291fs (Figure 3E,F; Table S2).

The smear specimens of peripheral blood were obtained every 1 to 2 months. The specimens showed that most of mice/D171N and mice/S291fs suffered from multilineage dysplasia characteristic of MDS. Erythroid dysplasia such as Howell-Jolly bodies, red cell polychromasia, and poikilocytosis (Figure 4A) were frequently detected in both mice. In BM specimens of morbid mice, orthochromatic giant erythroblasts and karyorrhexis were detected (Figure 4B). Erythroid dysplasia was more evident in mice/S291fs than in mice/D171N. As recently described in a mouse MDS model,[15] increase of red blood cell mean corpuscular volume (MCV) was also observed in most mice/D171N and mice/S291fs (Figure 3D; Table S2). Myeloid dysplasia such as the pseudo-Pelger-Huet anomaly (Figure 4C) was frequently detected in mice/D171N. Hypersegmented neutrophils (Figure 4D) and giant platelets (Figure 4F) were observed in 2 mice/D171N (mouse IDs 9 and 17). Collectively, AML1 mutants used in this study induced multilineage dysplasia, in particular in erythroid and myeloid lineages. Continuous pancytopenia was observed in 7 of 8 morbid mice/S291fs and 2 of 16 morbid mice/D171N, although BM of the morbid mice was not hypocellular but hypercellular or normocellular. Based on these findings, a final diagnosis was made by the ratio of blasts in the bone marrow according to the Bethesda proposals for classification of nonlymphoid hematopoietic neoplasms in mice.[41] As a result, MDS/AML was recognized in 13 of 16 morbid mice/D171N and in 5 of 8 morbid mice/S291fs, while MDS-RAEB was recognized in 2 of 16 morbid mice/D171N and 2 of 8 morbid mice/S291fs (Table S2). One mouse/D171N was diagnosed with AML at 4 months after transplantation because we did not examine to see if the MDS phase had preceded AML (mouse ID 5). The leukemic cells derived from either mice/D171N or mice/S291fs were serially transplantable. We confirmed the serial transplantability in 11 mice/D171N (mouse IDs 4, 6, 9, 12-15, 17, 20, 22, and 26) and 6 mice/S291fs (mouse IDs 52, 54-56, 58, and 60). Penetrance of serial transplantation was 100%, except for mouse IDs 9 and 17; that is, 33% and 50%, respectively. Mice that underwent serial transplantation showed more aggressive status than primary mice

Figure 3. Peripheral white blood cell counts of mice/D171N showed leukocytosis, while mice/ S291fs showed leukocytopenia. (A) Counts of white blood cells (WBCs) in PB. (B) Concentration of hemoglobin (Hg). (C) Counts of platelets (PLT). (D) Red cell MCV. (E,F) Weight of spleen and liver of morbid mice (mice/D171N or S291fs) or 1-year-old healthy mice (mice/WT or mock). Statistical differences were determined by 2-sample t test with Welch correction (*$P < .05$; **$P < .01$). Lane 1: mice/D171N without high expression of Evi1 in BM or not examined due to the lack of bone marrow samples (WBC, PLT, Hg, and MCV: n = 11; spleen: n = 5; and liver: n = 4). Lane 2: mice/D171N with high expression of Evi1 (n = 11). Lane 3: mice/S291fs (WBC, PLT, Hg, and MCV: n = 9; spleen and liver: n = 8). Lane 4: mice/WT (WBC, PLT, Hg, and MCV: n = 10; spleen and liver: n = 4). Lane 5: mice/mock (WBC, PLT, Hg, and MCV: n = 12; spleen: n = 6; and liver: n = 5).
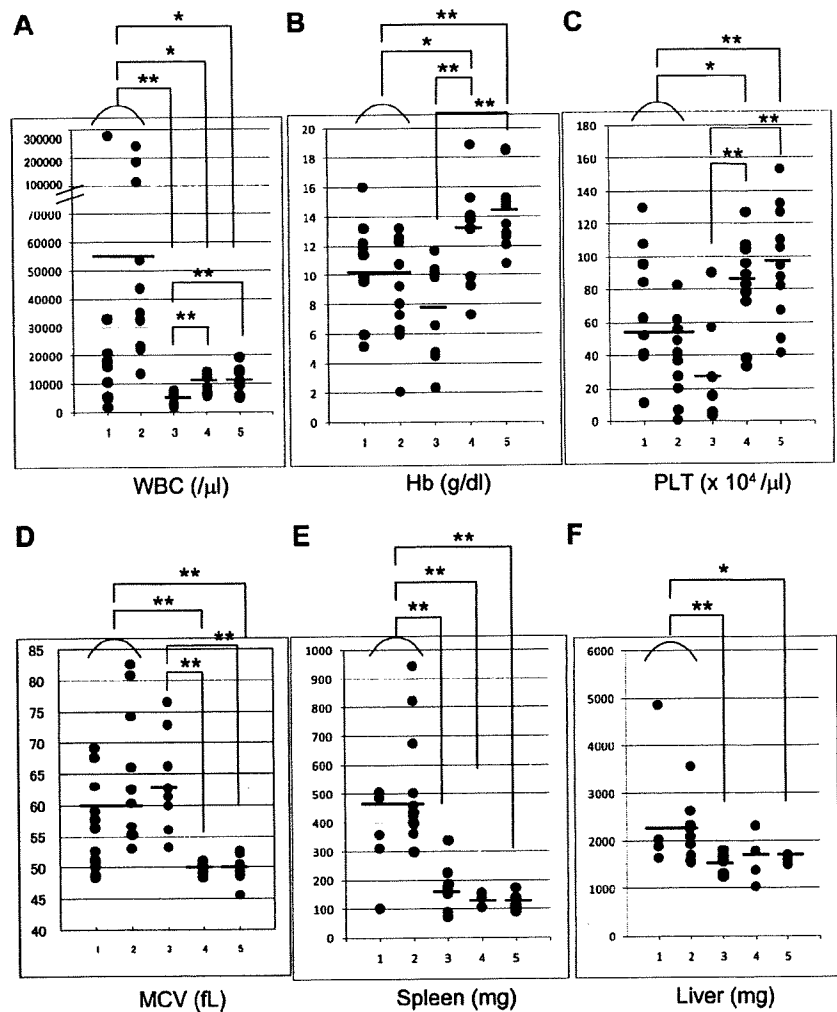
and died with shorter latencies. Hematologic parameters of mice that underwent serial transplantation are shown in Table S3.

In summary, the pattern and degree of multilineage dysplasia differed among the mice that underwent transplantation. Although both mice/D171N and mice/S291fs died of MDS and MDS/AML within 4 to 13 months after transplantation, a marked difference existed in terms of clinical symptoms, including hematopoietic or macroscopic findings.

### A distinct type of disease was identified in mice/D171N

Among the mice that underwent transplantation transduced with AML1-D171N, a distinct group was identified. GFP+ BM cells in 11 of 16 morbid mice/D171N (mouse IDs 4, 6, 7, 12-15, 19, 20, 22, and 26) displayed a similar phenotype, with high percentages of CD11b+ and B220+ cells (Figure 5; data not shown). All these mice/D171N showed dysplasia in myeloid and erythroid lineages for several months and died of MDS/AML with increased number of blasts, anemia, and, in some cases, thrombocytopenia (Table S2). These mice/D171N also showed severe hepatosplenomegaly (Figures 3E,F, 6A; Table S2), and histologic examination showed expansion of blasts and immature myeloid cells in the PB, BM, and spleen, and the invasion of these cells into hepatic portal areas in the liver and spaces among renal tubules in the kidney (Figure 6B,D,F). Giemsa staining of BM showed a high percentage of

blasts (Figure 6H), in accordance with a high percentage of both GFP/c-kit double-positive cells by flow cytometolic analysis.

In contrast, the remaining 4 morbid mice/D171N diagnosed as MDS (mouse IDs 9 and 11) or MDS/AML (mouse IDs 10 and 17) showed heterologous phenotypes of GFP+ BM cells (data not shown). Although mouse IDs 9 and 17 displayed hepatosplenomegaly like other mice/D171N, they exhibited leukocytopenia with fewer blasts.

AML1-D171N collaborated with Evi1 in inducing MDS/AML

We then asked why even the same point mutant of AML1 caused different phenotypes of MDS-RAEB and MDS/AML. We assumed the possibility that the integration of retroviruses influenced the outcomes in the BMT model. To explore this, we first performed Southern blot analysis of BM of the morbid mice. A single or several proviral integrations were confirmed (Figure 7A). Next, we used the bubble PCR method to identify the integrated sites.[7,44,45] A single or 2 integration sites were identified in each sample (Table 1). Interestingly, integrations near Evi1 site were found in 7 of 15 genomic DNA samples of BM cells derived from mice/D171N, but not from mice/S291fs. Moreover, retrospective examination revealed that these 7 mice presented nearly identical phenotypes, characterized by marked hepatosplenomegaly (Figure 6A), leukocytosis (Figure 3A), and biphenotypic surface markers (CD11b+
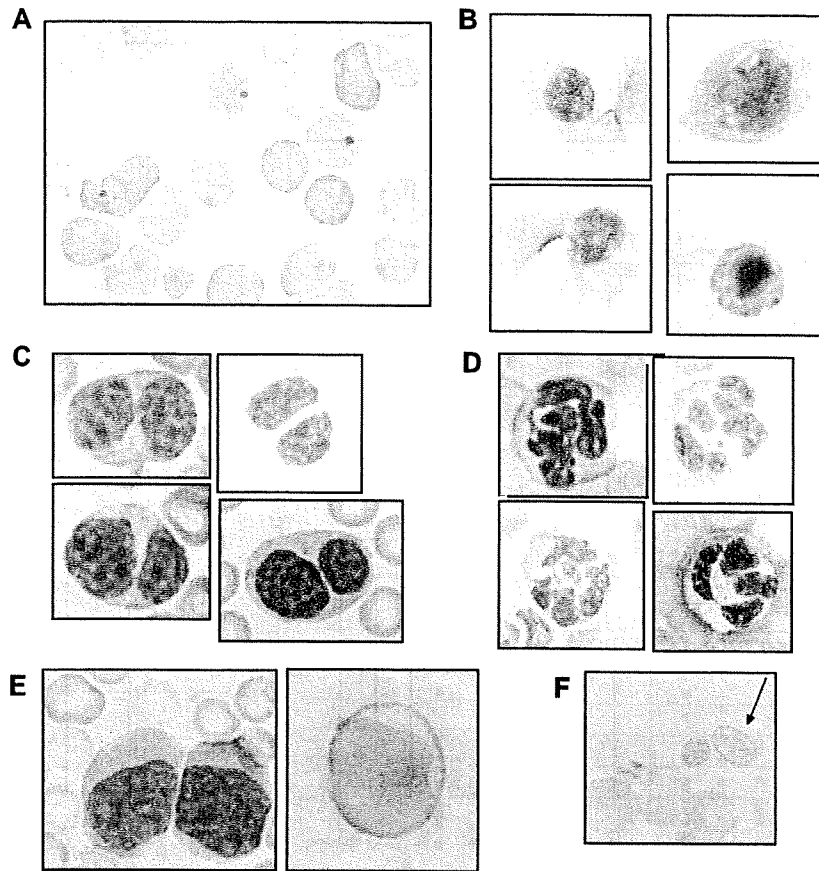
Figure 4. Multilineage dysplasia of hematopoietic cells in mice that received transplants of *AML1* mutants. Giemsa-stained PB smears obtained from mice/D171N or S291fs are shown. (A) Howell-Jolly body, polychromasia, and anisopoikilocytosis. (B) Orthochromatic giant erythroblast, karyorrhexis, and nuclear fragments. (C) Pseudo-Pelger-Huet anomaly. (D) Hypersegmented neutrophil. (E) Blasts in peripheral blood. (F) Giant platelet. Images were obtained with a BH51 microscope and DP12 camera (Olympus, Tokyo, Japan); objective lens, UPlanFl (Olympus); magnification, ×1000.

and B220⁺) of the leukemic cells (Figure 5), thus constituting a definite subgroup among mice/D171N. Southern blot analysis showed that all of the leukemic mice with high expression of Evi1 are monoclonal (except for mouse IDs 15 and 19), but the other leukemic mice without high expression of Evi1 are oligoclonal or have several integrations (Figure 7A). Noteworthy was the finding that the *Evi1* site was not identified from the genomic DNA samples of mice/S291fs, even though the *Evi1* site is a known common integration site of retroviruses.[31-38] These led us to postulate that Evi1 collaborated with AML1-D171N in inducing the distinct type of MDS/AML. To test this, we examined whether the expression of *Evi1* was enhanced in the BM cells in which the integration into an *Evi1* site was identified. Real-time PCR analysis demonstrated that the expression levels of *Evi1* were high in all the related samples (Figure 7C). Protein expression levels corresponded to mRNA expression levels of Evi1 (Figure 7D; data not shown). Interestingly, 4 samples derived from mice/D171N harboring no integration near *Evi1* also displayed significantly high expression levels of *Evi1* (mouse IDs 13, 19, 20, and 22), and the phenotypes of these mice were identical to those induced by AML1-D171N–transduced cells in which retroviruses were integrated into the *Evi1* site. In these cases, the expression of *Evi1* might have been enhanced secondarily by an unknown mechanism, or we simply failed to detect the integration site. The latter possibility was supported by the fact that multiple integrations were detected in these cases (Figure 7A; mouse IDs 13, 19, and 20). In any case, all the mice/D171N with enhanced expression of Evi1 in their BM cells displayed high percentages of blasts (Figure S1). We also examined whether the expression of MDS1/Evi1 was enhanced by the integration into an *Evi1* site. The *MDS1* gene is located approximately 240 kb upstream of Evi1, and MDS1/Evi1 is generated from the in-frame splicing of MDS1 to the second exon of Evi1.[36,43] Real-time

PCR analysis demonstrated that the expression levels of MDS1/Evi1 were low and were not significantly increased when compared with controls (data not shown). The integration sites of *Evi1* were focused on two regions (Table 1). One is 15 kb upstream of start site of *Evi1* (mouse IDs 12, 14, 15), and another is 107 kb upstream of start site of *Evi1* (mouse IDs 4, 6, 7, 26). Morishita et al reported that the retrovirus integrations had occurred near or in 5′ noncoding exons of *Evi1* gene.[31] The integration site at 15 kb upstream of the start site of *Evi1* that we found is near to the site they reported.

In vivo collaboration between *Evi1* and AML1-D171N

Next, we tested to see if *Evi1* expression collaborates with AML1-D171N in inducing leukemia in the BMT model. Cotransduction of AML1-D171N and Evi1 into BM cells resulted in rapid induction of the disease in the mice that underwent transplantation that was essentially identical with the disease that developed after a long latency in the mice/D171N (Figures 1E,5). In fact, all the mice displayed increased number of blasts in the PB within a month after the transplantation of BM cells transduced with Evi1/D171N. Southern blot analysis showed that these leukemic cells were polyclonal (Figure 7B). These results indicate that AML1-D171N and Evi1 collaborate to induce MDS/AML with a distinct phenotype. On the other hand, cotransduction of AML1-S291fs and *Evi1* into BM cells did not induce MDS/AML in 5 months (data not shown). In the present work, mice that received transplants of BM cell–transduced *Evi1* alone did not present any abnormalities in 5 months (Figure 1E).

Figure 5. AML1-D171N Induced a biphenotypic leukemia in concert with Evi1 in the BMT model. The dot plots show Ly5.1, Gr-1, CD11b, B220, CD3, CD41, c-kit, Sca-1, CD34, or Ter119 labeled with a corresponding PE-conjugated mAb versus expression of GFP. BM cells of morbid mice/D171N with high expression of *Evi1* (mouse IDs 6, 20, and 26) and those of morbid mice/D171N + *Evi1* (mouse IDs 302 and 305) displayed a similar pattern of surface markers, CD11b^{+} and B220^{+}.
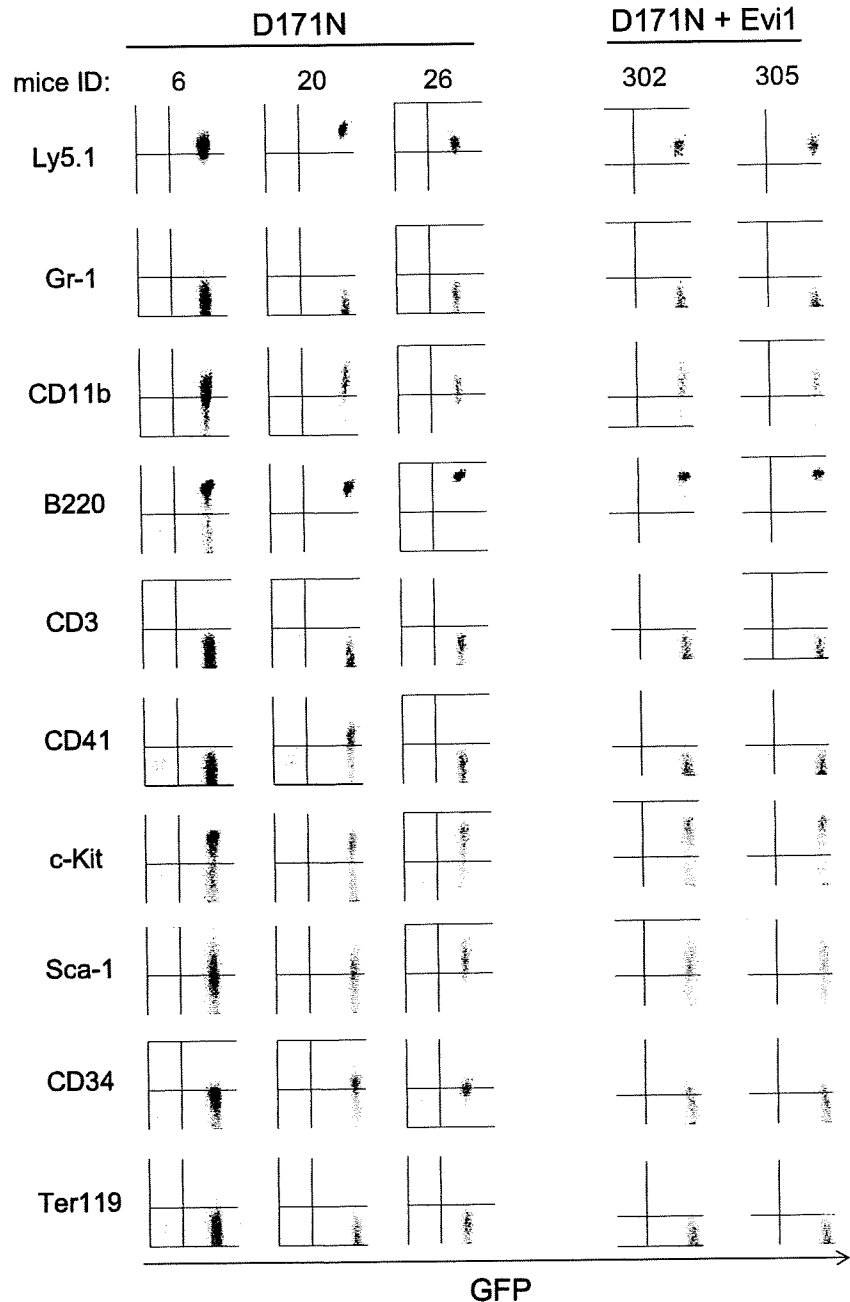
AML1-S291fs induced erythroid dysplasia with pancytopenia

In contrast to mice/D171N, most of mice/S291fs displayed remarkable erythroid dysplasia with continuous pancytopenia (Figures 3A-C,4A). A total of 2 of 8 mice/S291fs died of MDS-RAEB in which the percentage of blasts in the bone marrow was less than 20%, and 5 mice/S291fs developed MDS/AML. The mice displayed severe anemia but not leukocytosis in the PB, and the numbers of blasts were generally lower than those of MDS/AML mice transduced with AML1-D171N (Table S2). Surface markers of leukemic cells derived from mice/S291fs were different from those of mice/D171N (Figure S3).

We found integrations of the retrovirus in the intron of MN1 in 3 of 8 mice/S291fs (Table 1; mouse IDs 55, 56, and 58), and MN1 was overexpressed in the leukemic cells of these mice (Figure S2). The integration site was identical among these leukemic cells, indicating that leukemic cells of the 3 mice were derived from a single hematopoietic progenitor and that overexpression of MN1 induced expansion of the transduced stem cells during the 3-day culture period before the transplantation. Indeed, the mice with the integration at that MN1 site developed MDS/AML with shorter latencies (Table S2).

Discussion

We have established a mouse BMT model for MDS and MDS/AML using *AML1* mutants derived from patients with MDS,